Supporting Information for

Polyamine Promotes Electrochemical Reduction of CO_2 to HCOOH Catalyzed by Manganese Terpyridine dicarbonyls Complex

Rui Li,[a] Shuanglin He,[a,c] Fang Huang,[b] Ping Zhang,[a] Ying Xiong,[a] Rong Zhang,[c] Fei Li*[c] and Lin Chen*[a]*

[a] State Key Laboratory of Environment-Friendly Energy Material, School of Materials and Chemistry, Southwest University of Science and Technology, Mianyang 621010, P. R. China

[b] College of Chemistry, Chemical Engineering and Materials Science, Shandong Normal University, Jinan 250014, P. R. China

[c] State Key Laboratory of Fine Chemicals, Dalian University of Technology, Dalian 116024, P. R. China

Corresponding Authors

Email*: chenlin101101@aliyun.com

Email*: fanghuang@sdnu.edu.cn

Email*: lifei@dlut.edu.cn

Contents

1.Figue contents

2. Table Contents

3. Scheme Contents

4. Materials and Instruments

All manipulations for preparation and handling of organometallic complexes were carried out under Ar. All the solvents were used as received. Other commercially available chemicals such as $Mn(CO)_5Br$, $Pd(PPh_3)_4$, benzaldehyde, 1-(pyridin-2-yl)ethanone, potassium hydroxide, pyridine, toluene, potassium carbonate, anhydrous methanol and iodine were purchased from local suppliers and used as received. Water was deionized with the Millipore Milli-Q UF Plus system. Glass carbon disc (3 mm), Ag^+/Ag electrode and platinum wire were purchased from CHI for electrochemical studies.

NMR Spectra were collected with a varian INOVA 600 NMR spectrometer. Mass spectra were recorded with HP 1100 HPL/ESI-DAD-MS and Waters/Micromass LC/Q-TOF-MS instruments. Elemental analyses were performed with a Thermoquest-Flash EA 1112 elemental analyzer.

5. Electrochemistry Study Details

Cyclic voltammetry (CV): Cyclic voltammetry experiments were carried out in a three-electrode cell under high-purity Ar (99.999%) or CO_2 (99.99%) using CHI 760E potentiostat. The working electrode was a glassy carbon disc (diameter 3 mm) polished with 0.5-mm diamond pastes, then sonicated in ion-free water for 15 min and washed with MeCN prior to use. The reference electrode was a Ag^+/Ag (0.01 M $AgNO_3$) electrode and the counter electrode was platinum wire. Manganese complex concentrations were generally at 0.5 mM. A solution of 0.1 M $^nBu_4NPF_6$ (Fluka, electrochemical grade) in CH_3CN was used as supporting electrolyte, which was degassed by bubbling with dry Ar or CO_2 for 5 min before measurement. The catalytic experiments with CO_2 were performed in CO_2 saturated CH_3CN solution (about 0.28 M) with addition of a certain amount of anhydrous TFE. The scan rate is 100 mV/s. Ferrocene (Fc) was added as an internal reference in the end of each measurement to convert the measured potentials and all potentials given in this work are referred to $Fc^{+/0}$.

Controlled potential electrolysis experiments (CPE): Controlled potential electrolysis experiments were carried out in a custom 18 mL cell designed in our laboratory. The setup included a glassy carbon cell working electrode, graphite rod counter electrode separated from the solution by a porous glass frit, and $Ag/AgNO_3$ pseudoreference electrode. For the catalytic electrolysis studies, the cell was charged with Mn catalyst (0.5 mM) and TFE (1.5 M) in 0.1 M tetra-n-butylammonium hexafluorophosphate solution (CH_3CN). Gas products were quantified by analyzing 50 μL aliquots of the headspace on a Beifen 6890A Series gas chromatograph. The partial pressure of H_2/CO in the headspace was determined by comparison to gas standard samples. Henry's Law was used to calculate the total H_2/CO production, given as the sum of headspace and dissolved H_2/CO.

Typical Experimental Conditions: Purity of the electrolyte medium was confirmed over the available electrochemical window through background scans taken prior to addition of analyte. 0.5 mM of catalist and 1.5 M of TFE were weighed into an 18 mL glass vial and dissolved in 8 mL of a supporting electrolyte solution (0.1 M $[^nBu_4N][PF_6]/CH_3CN$). The solution was saturated with CO_2 by bubbling CO_2 into the electrolyte for about 30 min prior to the experiment.

6. Product Analysis

The gas products in the headspace of the cell were analyzed by a gas chromatograph (GC, Beifen 6890A s), which was equipped with TCD and FID detectors. Gas sample H_2, CH_4 and CO are separated by stainless-steel column packed with molecular sieves (5 Å × 3 m) and the carrier gas is Ar (flow rate = 35 mL·min^{-1}). The TCD detector was used to detect H_2 at a detection limit of 1 ppm. The FID detector was furnished with a methanizer to detect CH_4 and CO at a detection limit of 0.5 ppm. Gas chromatography calibration curves were made by sampling known volumes of H_2, CH_4 and CO gas. Other gas samples such as ethyene and ethanal could be separated by Porapak N column and detected by FID. The operating temperatures of the injection port, the oven/column, and detector were 50 °C, 50 °C and 380 °C, respectively. Aliquots (50 μL) of the gas headspace were injected into the GC in the end of electrolysis to analyze the gas products formed. The gas path is shown in the figure below.

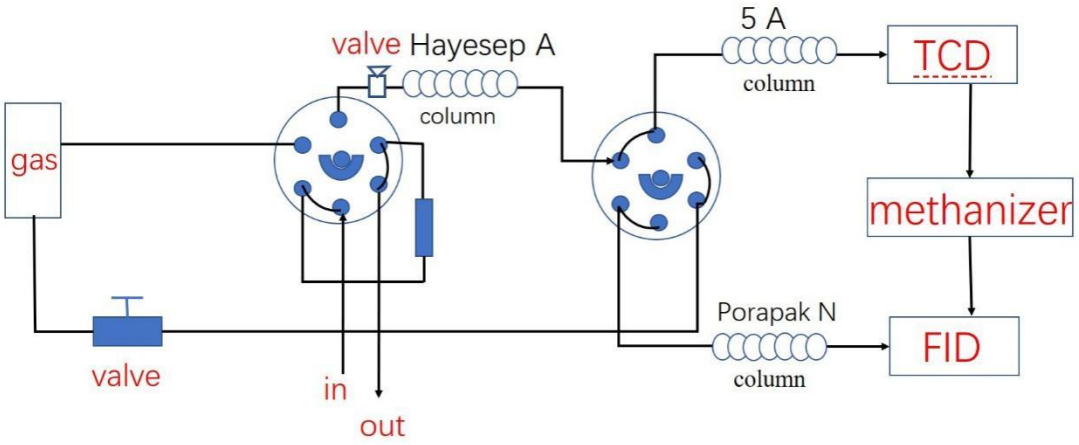

The liquid product (HCOOH) in the resulting electrolyte was detected by using ion chromatograph (Shenghan ICS-380), which was equipped with an electrical conductivity detector and an ionic exchange column. The ion chromatographic measurements were made with 1 M K_2CO_3/$KHCO_3$ aqueous solution as flowing phase in a negative ion model and with potassium formate as external stantard. Before measurement, the resulting electrolyte was treated with 1 M K_2CO_3/$KHCO_3$ aqueous solution for 1 h to convert formic acid and methyl formate in the solution to potassium formate. The isotope labeled formic acid H^{13}COOH obtained from $^{13}CO_2$ reduction was detected by GC-MS spectra measured on an Agilent 7890A GC instrument equipped with a

capillary column: HP-PLOT (30 m x 320 um), which was connected to an Agilent 7000 MS spectrometer with a triple quad detector.

7. Calculation for Faradaic Efficiency

$$Faradaic\ yield\ product\ (\%) = 100 \times n_{prod}./\ (Q / F / 2)$$

Where F is the Faraday constant ($C \cdot mol^{-1}$), n_{prod} (mol) is the amount of CO measured in the headspace, and Q (C) is the charged passed during electrolysis.

Fourier-Transform Infrared Reflectance Spectroelectrochemistry (FTIR-SEC)

A homemade FTIR-SEC instrument was used for this study. The cell consists of a glass carbon working electrode (10 mm), a Pt counter (15 mm × 30 mm) electrode, and a $Ag/AgNO_3$ reference electrode and a CaF_2 plate as the optical window. The IR beam is directed to focus on the working electrode through the optical window, where it is reflected and ultimately directed to the Bruker Vertex 80 detector. The dry CH_3CN solution (0.2 M TBAP) prepared under an atmosphere of Ar is used as the electrolyte.

8. Experiment section

General methods for preparing the precursors and target ligands in this article.

6-Precursor: The procedure was slightly modified according to the literature (Chotalia R, et al. *Dalton Trans*., 1996, **389**, 4207-4216). Taking the synthesis of compound B as an example. Prepare a 150 mL beaker with an integrated magnetic stir bar, and then add 2-acetyl-6-methylpyridine (1 equiv), benzaldehyde (1.2 equiv), and ice methanol (100 mL). While stirring, add a 2 M KOH aqueous solution (10 mL) dropwise, and then stir the mixture at room temperature for 3 hours, resulting in the precipitation of a yellowish-white powder. Filter the mixture and wash with ice methanol to obtain a white powder, which is then air-dried. Take the obtained white powder (1 equiv) and combine it with 2-pyridyl-2-oxoethylpyridinium iodide (1.2 equiv), ammonium acetate (10 equiv), and anhydrous methanol (30 mL) in a dry round-bottom flask. Reflux the mixture at 80°C for 6 hours. After the reaction, cool the mixture to room temperature, filter, and wash with ice methanol to obtain a grayish-black solid powder, which is then air-dried. Finally, separate and purify the product using column chromatography (yield: 56%).

Precursor

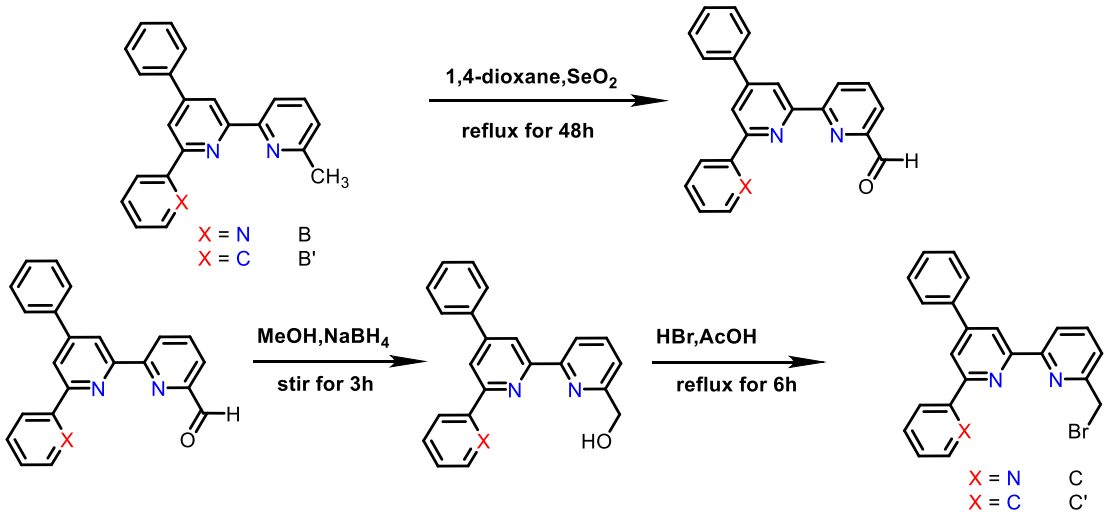

Scheme S 1 preparation of precursor **C, C'**.

4'-phenyl-[2,2':6',2''-terpyridine]-6-carbaldehyde(**B**),

4',6'-diphenyl-[2,2'-bipyridine]-6-carbaldehyde,(**B'**)

6-(bromomethyl)-4'-phenyl-2,2':6',2''-terpyridine(**C**) and

6'-(bromomethyl)-4,6-diphenyl-2,2'-bipyridine(**C'**) was prepared with a modified reported method.

(Ding D, et al. *Tetrahedron Lett.*, 2013, **54**, 5211–5213.) Taking the synthesis of compound C as an example. To a mixture of SeO_2 (3.33 g, 25 mmol) and dioxane (25 mL), a solution of 6-Methyl-4'-phenyl-2,2':6',2"-terpyridine (6.46 g, 20.0 mmol) dissolved in dioxane (30 mL) was added dropwise at 65 ℃. After the addition was complete (30 min), the mixture was reflux for 48h at 105℃. After cooled to the room temperature, the solid was filtered out and the solvent of the filtrate removed by rotary evaporator. leaving an Light Yellow residue. The catalyst residue was removed by passing through a short silica gel column with dichloromethane as the eluent. After removing the solvent under reduced pressure, 4'-phenyl-[2,2':6',2"-terpyridine]-6-carbaldehyde (4.38 g, 13.0 mmol, yield: 65%) was obtained.

The obtained compound 4'-phenyl-[2,2':6',2"-terpyridine]-6-carbaldehyde(3.37 g, 10.0mmol) was dissolved in 30 mL of ice-cold methanol. Sodium borohydride (0.45 g,12.0mmol) was added slowly and in portions to the reaction apparatus. After the apparatus naturally warmed to room temperature, the reaction was allowed to proceed for an additional 3h during which a white solid precipitated. Upon completion of the reaction, the mixture was filtered, and the residue was collected and washed with ice-cold methanol, yielding (4'-phenyl-[2,2':6',2"-terpyridin]-6-yl)methanol (2.88 g, 8.5 mmol, yield: 85%) .

To the reaction apparatus containing solid sample (4'-phenyl-[2,2':6',2"-terpyridin]-6-yl)methanol(2.72 g,8.0 mmol), 8 mL of 35% HBr/AcOH (hydrobromic acid in acetic acid) was added. The mixture was refluxed and stirred for 6 hours, during which the solid sample dissolved, and the solution gradually turned from a pale yellow to a dark brown color. After the reaction was completed, the apparatus was allowed to cool naturally to room temperature, and 10 mL of ethyl acetate was added to the mixture. The resulting solution was stirred for 10 minutes, leading to the precipitation of a solid. The solid was collected by filtration and further purified by recrystallization using ethyl acetate. The final product was obtained in a yield of 6-(bromomethyl)-4'-phenyl-2,2':6',2"-terpyridine (2.41 g 6.0 mmol, yield: 75%).

Synthesis of ligand R1

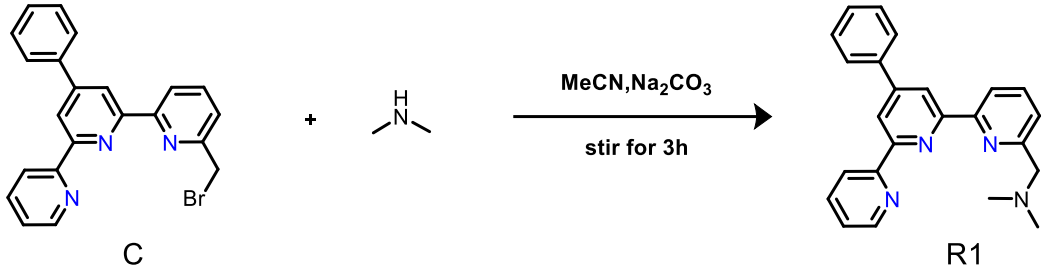

Scheme S 2 preparation of target ligand **R1**.

R1 was obtained according to the procedure described in the literature. (Wang J, et al. *Dalton Trans.*, 2024, **53**, 5222–5231.). 6-(bromomethyl)-4'-phenyl-2,2':6',2"-terpyridine (0.402 g, 1 mmol) was dissolved in Acetonitrilel (5 mL). A 40% (w/w) aqueous solution of dimethylamine (5.0 ml, 10.0 mmol) was added dropwise. The mixture was stir at room temprature for 1 h, the solvent was removed under reduced pressure. To deprotonate the compound, the white residue was dissolved in aqueous solution of NaOH (3 M, 20 ml). The solution was extracted with CH_2Cl_2 (3 × 10 ml). The organic layers were combined, dried under anhydrous sodium sulfate and the solvent was removed under reduced pressure. The residue was dried under high vacuum and the ligand was obtained as bright white solid (0.31 g, 0.84 mmol, yield: 84%).^{1}H NMR (600 MHz, DMSO) δ 8.77 (1H, d), 8.73 – 8.64 (3H, m), 8.55 (1H, d), 8.10 – 7.98 (2H, m), 7.95 – 7.85 (2H, m), 7.59 (5H, dt), 3.70 (2H, s), 2.27 (6H, s).

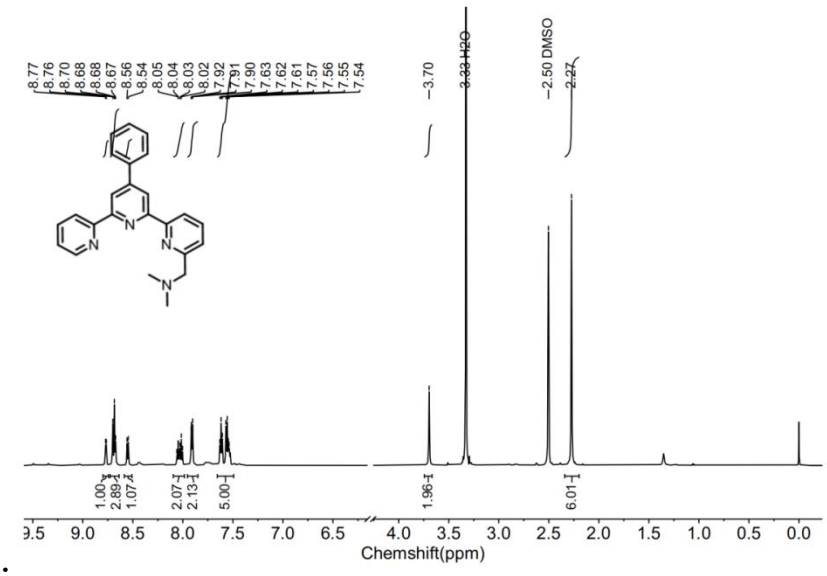

Figure S 1 ^{1}H NMR (DMSO, 600 MHz) spectrum of **R1**.

Synthesis of ligand R2

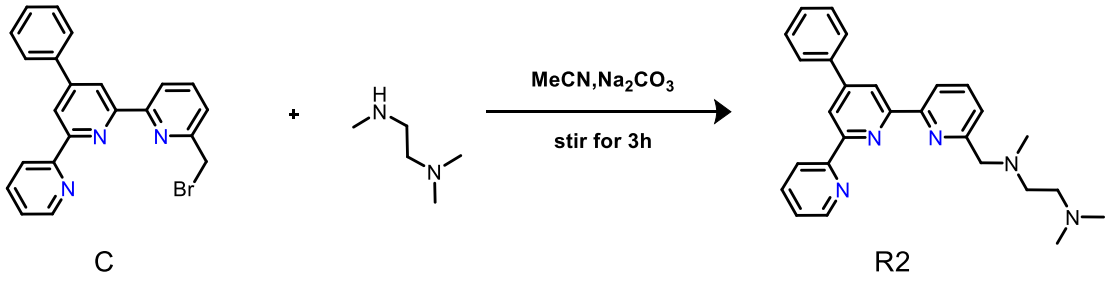

Scheme S 3 preparation of target ligand **R2**.

The procedure was slightly modified according to the literature. (Chai Y, et al. *Chem. Commun.*, 2014, **50**, 11668–11671.) 6-(bromomethyl)-4'-phenyl-2,2':6',2''-terpyridine (0.804 g, 2 mmol) was dissolved in Acetonitrilel (5 mL). A N^1,N^1,N^2-trimethylethane-1,2-diamine (0.25ml, 2.4 mmol) was added dropwise. The mixture was stir at room temprature for 2 h, the solvent was removed under reduced pressure. To remove the starting materials and by-products, the white residue was dissolved in a weakly acidic aqueous solution. The mixture was then extracted with dichloromethane, and the aqueous phase was collected. Subsequently, the pH of the aqueous phase was adjusted to weakly basic conditions. The resulting solution was extracted again with dichloromethane, and the organic phase was collected, dried under anhydrous sodium sulfate and the solvent was removed under reduced pressure. The residue was dried under high vacuum and the ligand was obtained as bright white solid (0.63 g, 1.49 mmol, yield: 75%): ^{1}H NMR (600 MHz, $CDCl_3$) δ 8.74 (2H, d), 8.70 – 8.64 (2H, m), 8.59 (1H, d), 7.94 – 7.85 (4H, m), 7.57 – 7.46 (4H, m), 7.37 (1H, ddd), 3.94 (2H, s), 3.20 – 3.09 (4H, m), 2.79 (6H, s), 2.47 (3H, s).

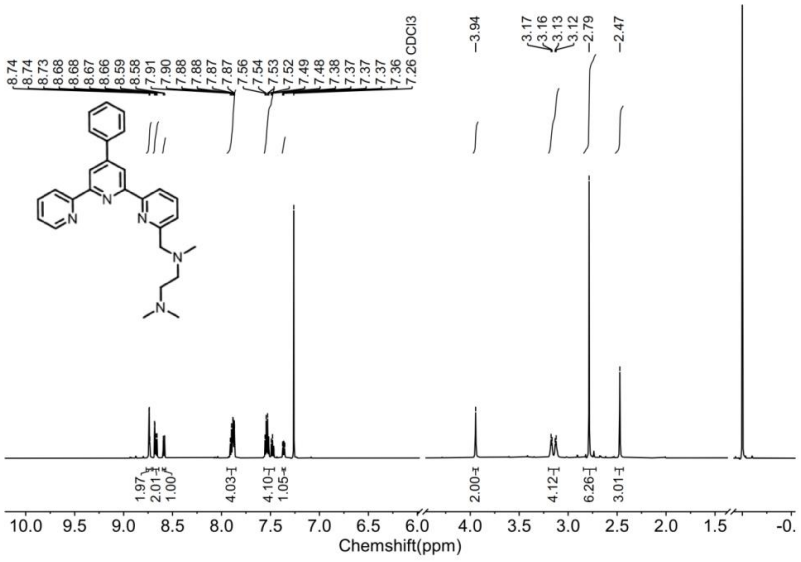

Figure S 2 ^{1}H NMR (Chloroform, 600 MHz) spectrum of **R2**.

Synthesis of ligand R3

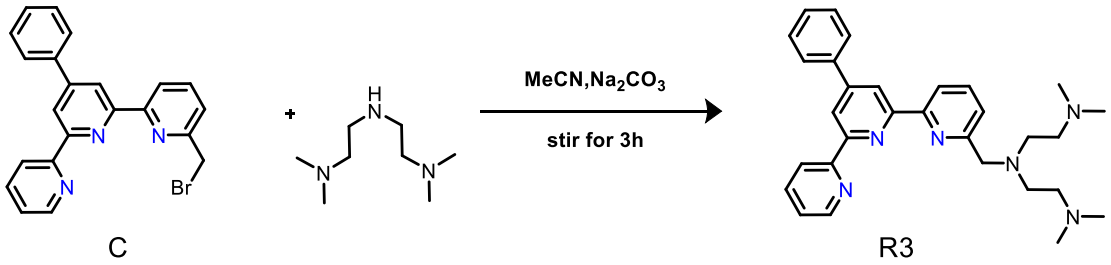

Scheme S 4 preparation of target ligand **R3**.

6-(bromomethyl)-4'-phenyl-2,2':6',2''-terpyridine (0.804 g, 2 mmol) was dissolved in Acetonitrilel (5 mL). A N1,N1-dimethyl-N2-(2-(methylamino)ethyl)ethane-1,2-diamine (0.35ml, 2.4 mmol) was added dropwise. The mixture was stir at room temprature for 2 h, the solvent was removed under reduced pressure. To remove the starting materials and by-products, the white residue was dissolved in a weakly acidic aqueous solution. The mixture was then extracted with dichloromethane, and the aqueous phase was collected. Subsequently, the pH of the aqueous phase was adjusted to weakly basic conditions. The resulting solution was extracted again with dichloromethane, and the organic phase was collected, dried under anhydrous sodium sulfate and the solvent was removed under reduced pressure. The residue was dried under high vacuum and the ligand was obtained as bright white solid (0.59 g, 1.24 mmol yield: 62%):^{1}H NMR (600 MHz, $CDCl_3$) δ 8.73 (2H, q), 8.71 – 8.64 (2H, m), 8.55 (1H, d), 7.92 – 7.83 (4H, m), 7.56 – 7.45 (4H, m), 7.38 – 7.34 (1H, m), 3.98 (2H, s), 2.98 – 2.64 (8H, m), 2.40 (12H, d).

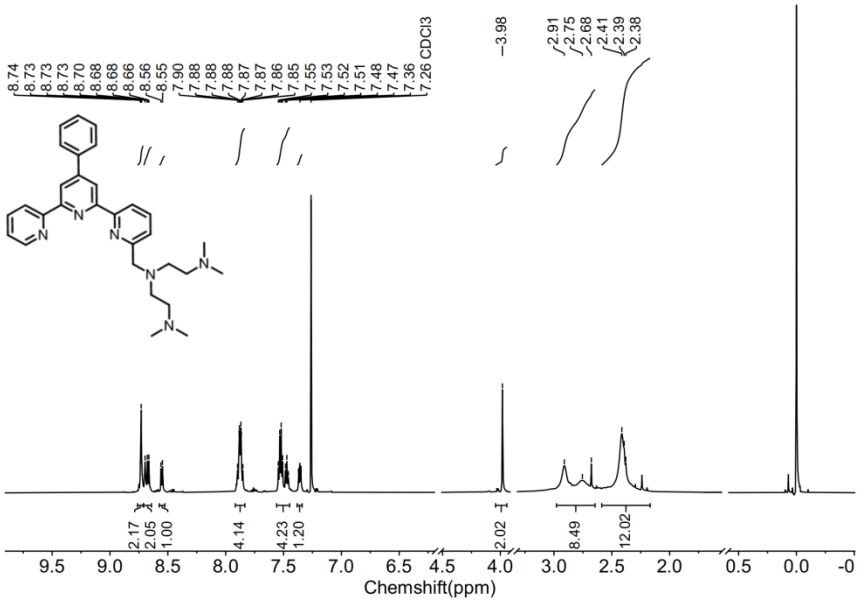

Figure S 3 ^{1}H NMR (Chloroform, 600 MHz) spectrum of **R3**.

Synthesis of ligand R4

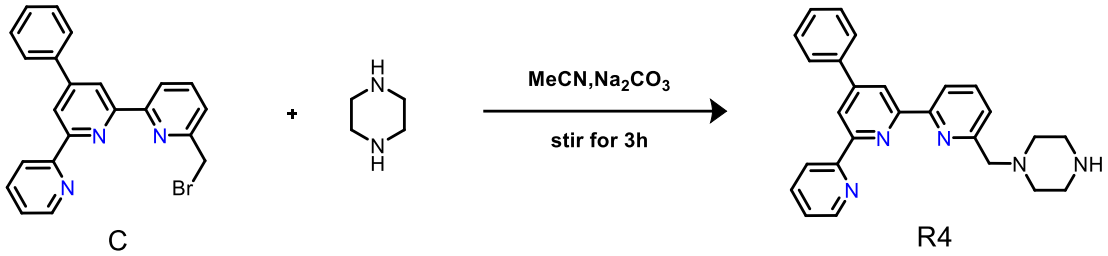

Scheme S 5 preparation of target ligand **R4**.

Piperazine (0.1 g, 1.2 mmol) was dissolved in MeCN (10 mL), and then a MeCN solution (5 mL) of 6-(bromomethyl)-4'-phenyl-2,2':6',2''-terpyridine (0.402 g, 1.0 mmol) was slowly added dropwise to the reaction solution at 0°C. After the addition was completed, the reaction was continued at 0°C for 1 hour. After the reaction was completed as determined by TLC, the mixture was washed several times with a saturated sodium bicarbonate solution, dried over anhydrous sodium sulfate, The solution was concentrated in vacuo to afford the title compound (0.37 g, 0.9 mmol, yield: 90%) as a viscous yellow oil. ^{1}H NMR (600 MHz, $CDCl_3$) δ 8.76 – 8.70 (3H, m), 8.66 (1H, dd), 8.57 (1H, d), 7.94 – 7.81 (4H, m), 7.57 – 7.43 (4H, m), 7.38 – 7.32 (1H, m), 3.88 (2H, s), 3.65 (1H, s), 3.27 (4H,d), 2.93 (4H, s), 1.02 (2H, t).

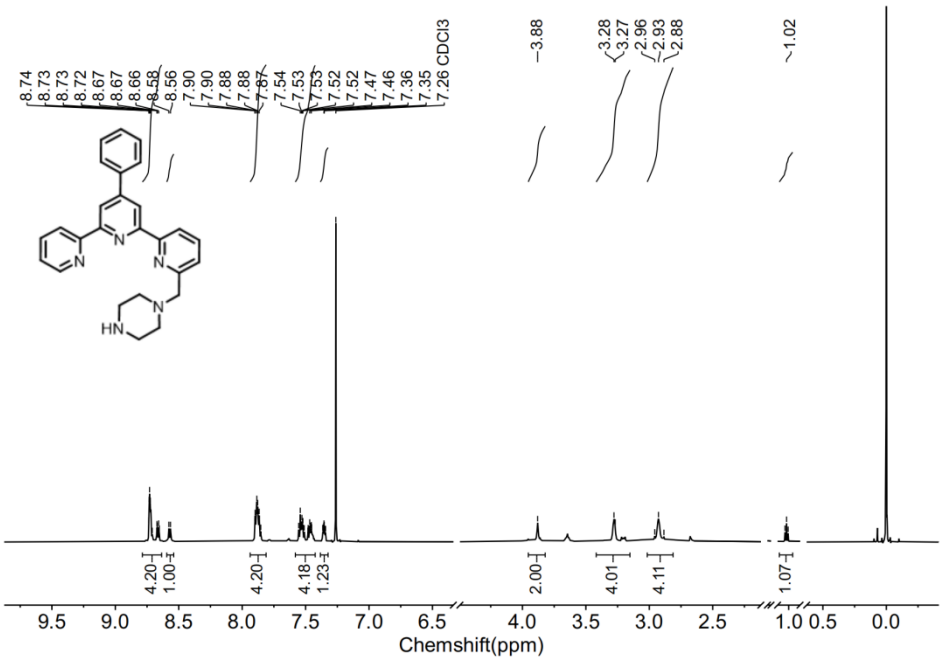

Figure S 4 ^{1}H NMR (Chloroform, 600 MHz) spectrum of **R4**.

Synthesis of ligand R5

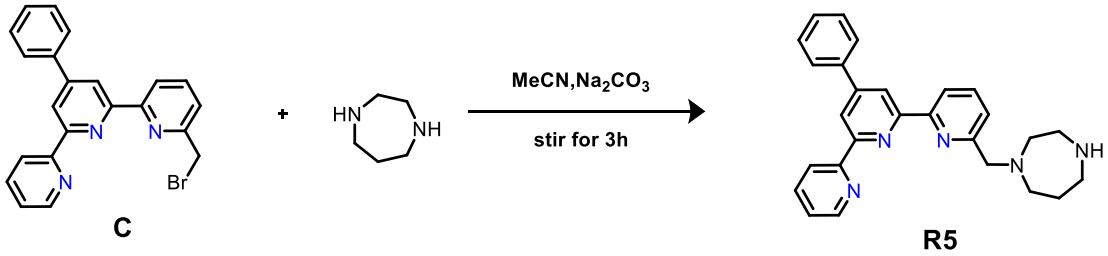

Scheme S 6 preparation of target ligand **R5**.

Homopiperazine (0.12 g, 1.2 mmol) was dissolved in MeCN (10 mL), and then a MeCN solution (5 mL) of 6-(bromomethyl)-4'-phenyl-2,2':6',2"-terpyridine (0.402 g, 1.0 mmol) was slowly added dropwise to the reaction solution at 0°C. After the addition was completed, the reaction was continued at 0°C for 1 hour. After the reaction was completed as determined by TLC, the mixture was washed several times with a saturated sodium bicarbonate solution, dried over anhydrous sodium sulfate, The solution was concentrated in vacuo to afford the title compound (0.37 g, 0.88 mmol, yield: 88%) as a viscous white solid. ^{1}H NMR (600 MHz, DMSO) δ 8.77 (1H, d), 8.76 – 8.67 (3H, m), 8.52 (1H, d), 8.07 – 7.99 (2H, d), 7.94 – 7.88 (2H, m), 7.65 – 7.51 (5H, m), 3.93 (2H, s), 3.30 (2H, s), 2.85 (2H, t), 2.79 (3H, dt), 2.73 – 2.65 (2H, m), 1.74-1.70 (2H, p).

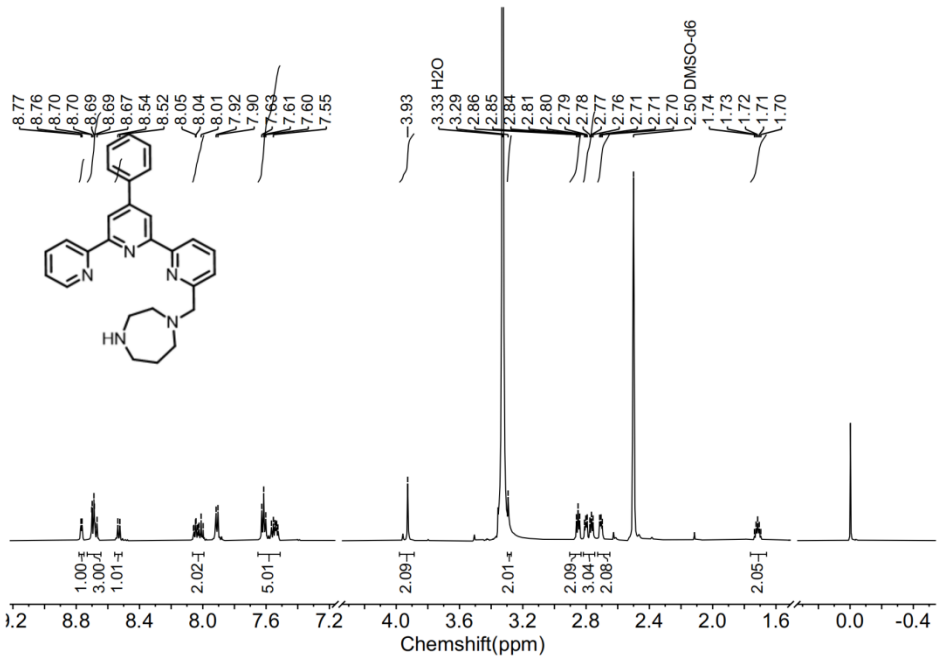

Figure S 5 ^{1}H NMR (DMSO, 600 MHz) spectrum of **R5**.

Synthesis of ligand R6

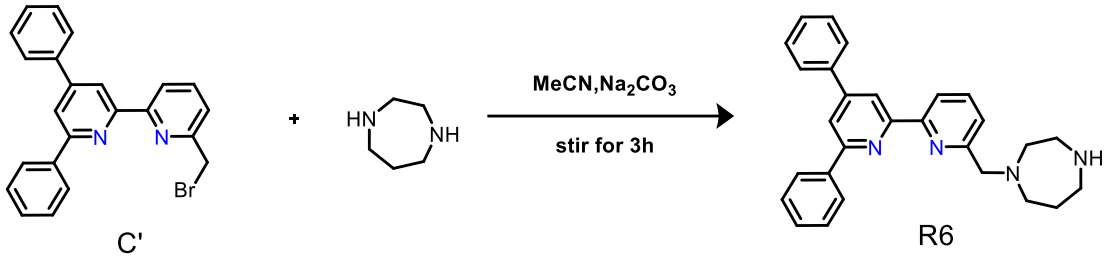

Scheme S 7 preparation of target ligand **R6**.

According to the Scheme S 6.for the synthesis of target ligand. Homopiperazine (0.1 g, 1.0 mmol) was dissolved in MeCN (10 mL), and then a MeCN solution (5 mL) of 6'-(bromomethyl)-4,6-diphenyl-2,2'-bipyridine (0.401 g, 1.0 mmol) was slowly added dropwise to the reaction solution at 0°C. After the addition was completed, the reaction was continued at 0°C for 1 hour. After the reaction was completed as determined by TLC, the mixture was washed several times with a saturated sodium bicarbonate solution, dried over anhydrous sodium sulfate, The solution was concentrated in vacuo to afford the title compound (0.38 g, 0.9 mmol, yield: 90%) as a viscous white solid.^{1}H NMR (600 MHz, $CDCl_3$) δ 8.62 (1H, d), 8.54 (1H, d), 8.21 (2H,

d), 7.97 (1H, d), 7.88 – 7.78 (3H, m), 7.59 – 7.51 (5H, m), 7.49 – 7.43 (2H, m), 3.99 (2H, s), 3.21 (2H, t), 3.17 – 3.11 (2H, m), 2.98 – 2.94 (2H, m), 2.88 (3H, t), 2.00 (2H, t).

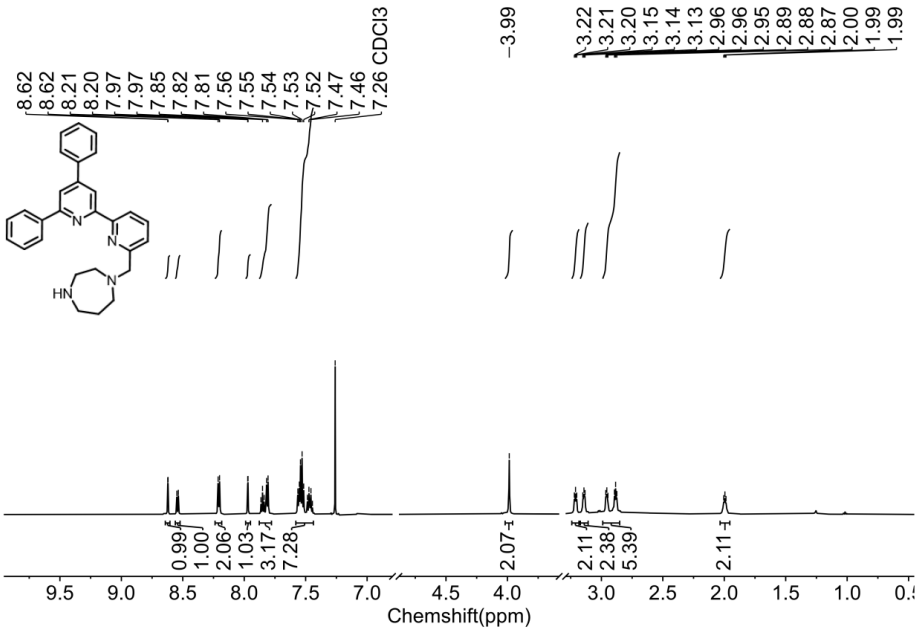

Figure S 6 ^{1}H NMR (Chloroform, 600 MHz) spectrum of **R6**.

Synthesis of complexes 1p

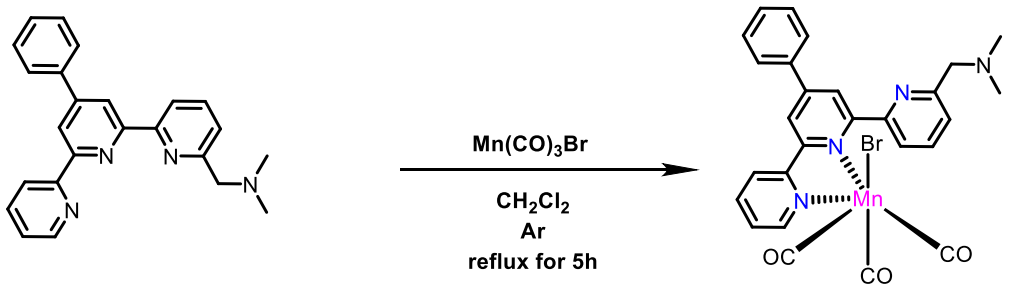

Scheme S 8 preparation of target complex **1p**.

Preparation of complexes **1p**. Compound $Mn(CO)_5Br$ (0.20 g, 0.72 mmol) was added to a degassed CH_2Cl_2 solution (5 mL) of 1 equiv **R1** (0.26 g, 0.72 mmol). The resulting orange solution was heated to reflux for 5 h under argon, then allowed to cool to room temperature before filtration. The filtrate was collected and concentrated, then washed with Et_2O and dried in vacuo to afford orange product (0.32 g, 0.55 mmol, yield: 77%). The following were observed for the mixture of atropisomers: ^{1}H NMR (600 MHz, DMSO) δ 9.29 – 9.17 (1H, m), 9.15 – 9.06 (1H, m), 9.01 (1H, m), 8.79 – 8.67 (1H, m), 8.63 – 8.49 (1H, m), 8.29 (2H, ddd), 8.22 – 8.10 (1H, m), 8.05

(1H, dt), 7.98 – 7.67 (3H, m), 7.60 (2H, dt), 3.68 (2H, d), 3.08 – 2.79 (3H, m), 2.36 – 2.14 (3H, m); IR (KBr, Figure S 19) ν_{CO}: 2021 (s), 1927 (s), 1913 (s) cm^{-1}; Anal. Calcd for 1p, $C_{27}H_{22}BrMnN_4O_3$: C, 55.40; H, 3.79; N, 9.57; found: C, 55.35; H, 3.85 N, 9.58; MS (TOF-ES): m/z = 500.0408/502.0391 $[M - 3CO]^+$, m/z = 421.1225/422.1225 $[M - 3CO - Br^-]^+$.

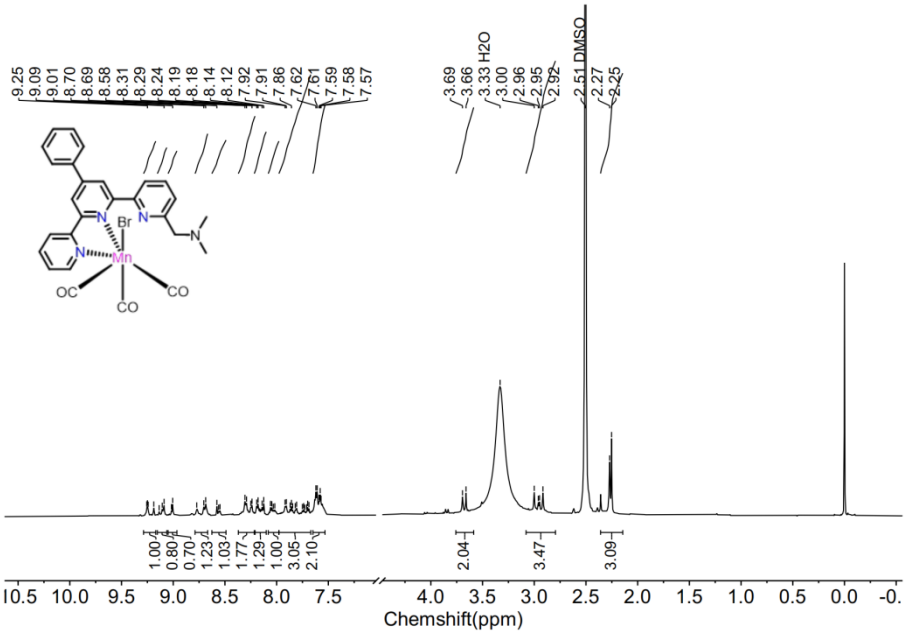

Figure S 7 ^{1}H NMR (DMSO, 600 MHz) spectrum of **1p**.

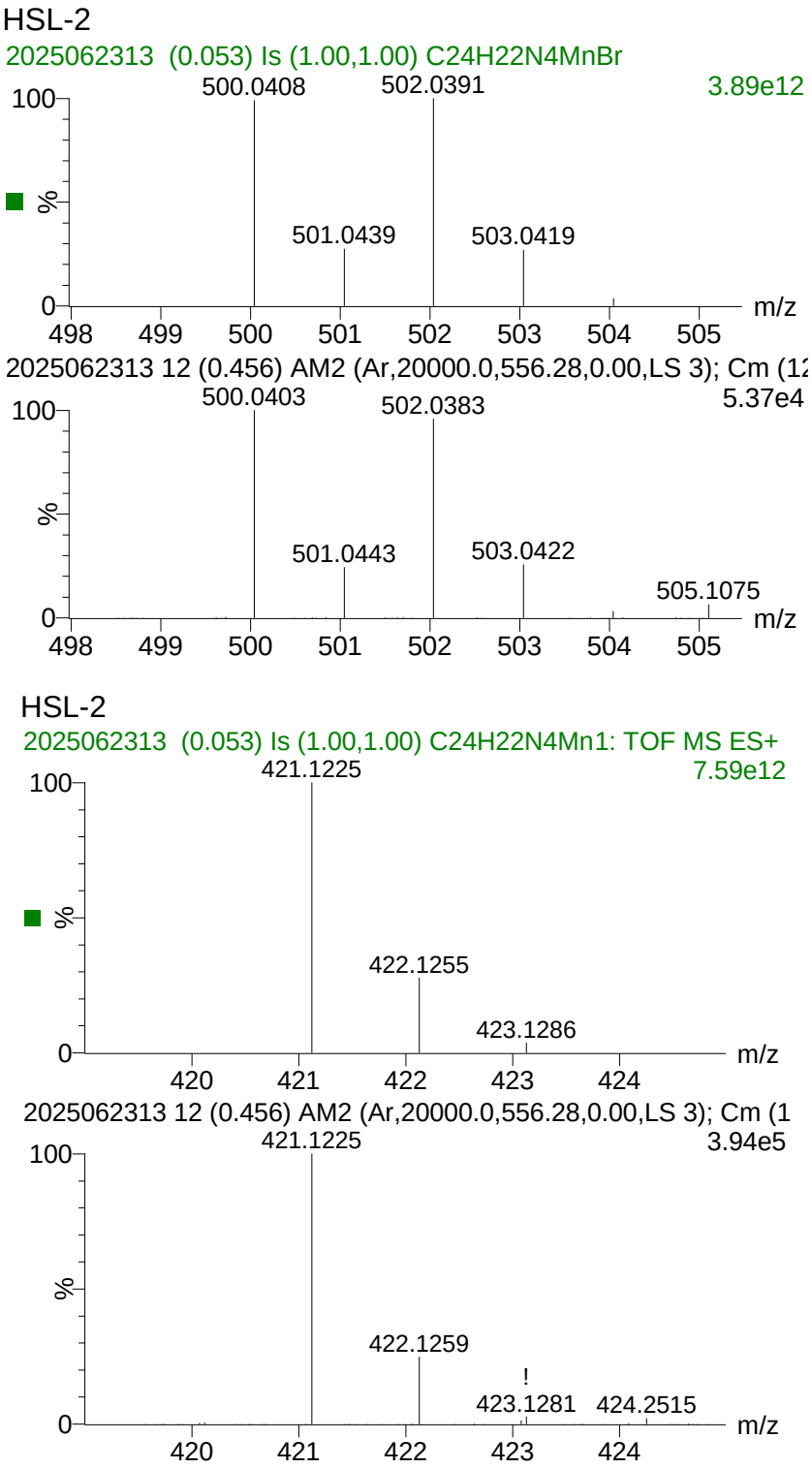

Figure S 8 high resolution mass spectrum of **1p**.

Synthesis of complexes 2p

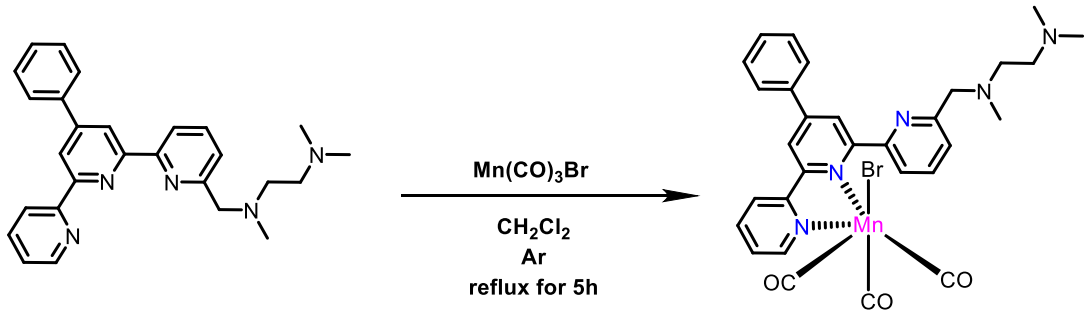

Scheme S 9 preparation of target complex **2p**.

Preparation of complexes **2p**. Compound $Mn(CO)_5Br$ (0.20 g, 0.72 mmol) was added to a degassed Dichloromethane solution (5 mL) of 1 equiv **R2** (0.30 g, 0.72 mmol). The resulting orange solution was heated to reflux for 5 h under argon, then allowed to cool to room temperature before filtration. The filtrate was collected and concentrated, then washed with Et_2O and dried in vacuo to afford orange product (0.34 g, 0.53 mmol, yield: 73%). The following were observed for the mixture of atropisomers:^{1}H NMR (600 MHz, DMSO) δ 8.90 (1H, s), 8.78 (1H,d), 8.46 (1H, d), 8.31 (2H, q), 8.15 (2H, d), 8.04 – 7.78 (4H, m), 7.70 – 7.49 (4H, m), 3.24 (2H, d), 2.67 (4H, d), 2.49 – 2.23 (5H, m), 2.01 (2H,d), 1.89 (2H,s).; IR (KBr, Figure S 19) νCO: 2026 (s), 1930(s), 1924 (s) cm-1; Anal. Calcd for **2p**, $C_{30}H_{29}BrMnN_5O_3$: C, 56.09; H, 4.55; N, 10.90; found: C, 56.18; H, 4.58; N, 10.88; MS (TOF-ES): m/z = 563.1754/562.1709 $[M - Br^-]^+$, m/z = 479.1846/478.1817 $[M - Br^- - 3CO]^+$.

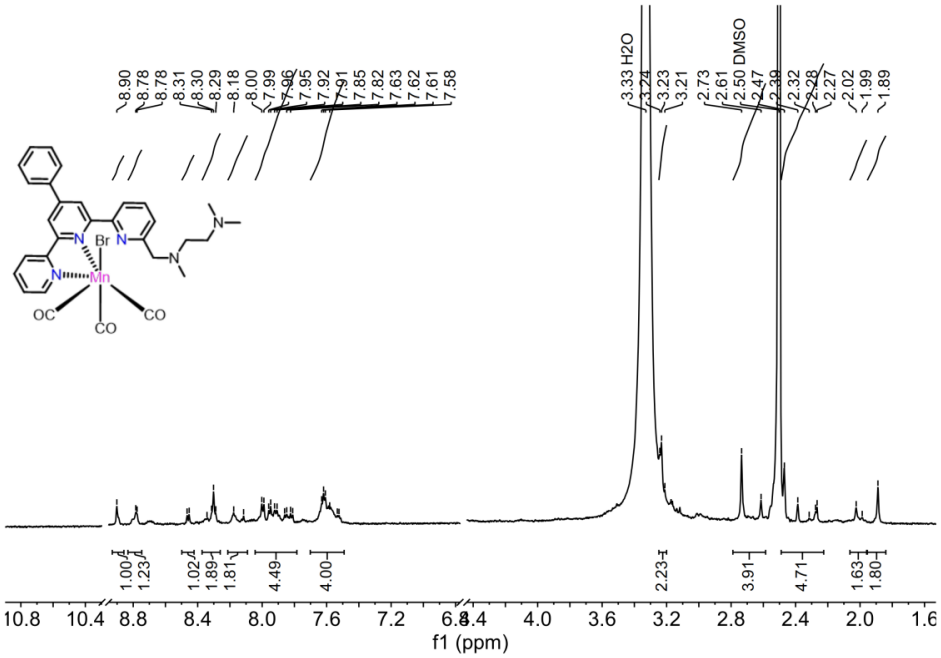

Figure S 9 ^{1}H NMR (DMSO, 600 MHz) spectrum of **2p**.

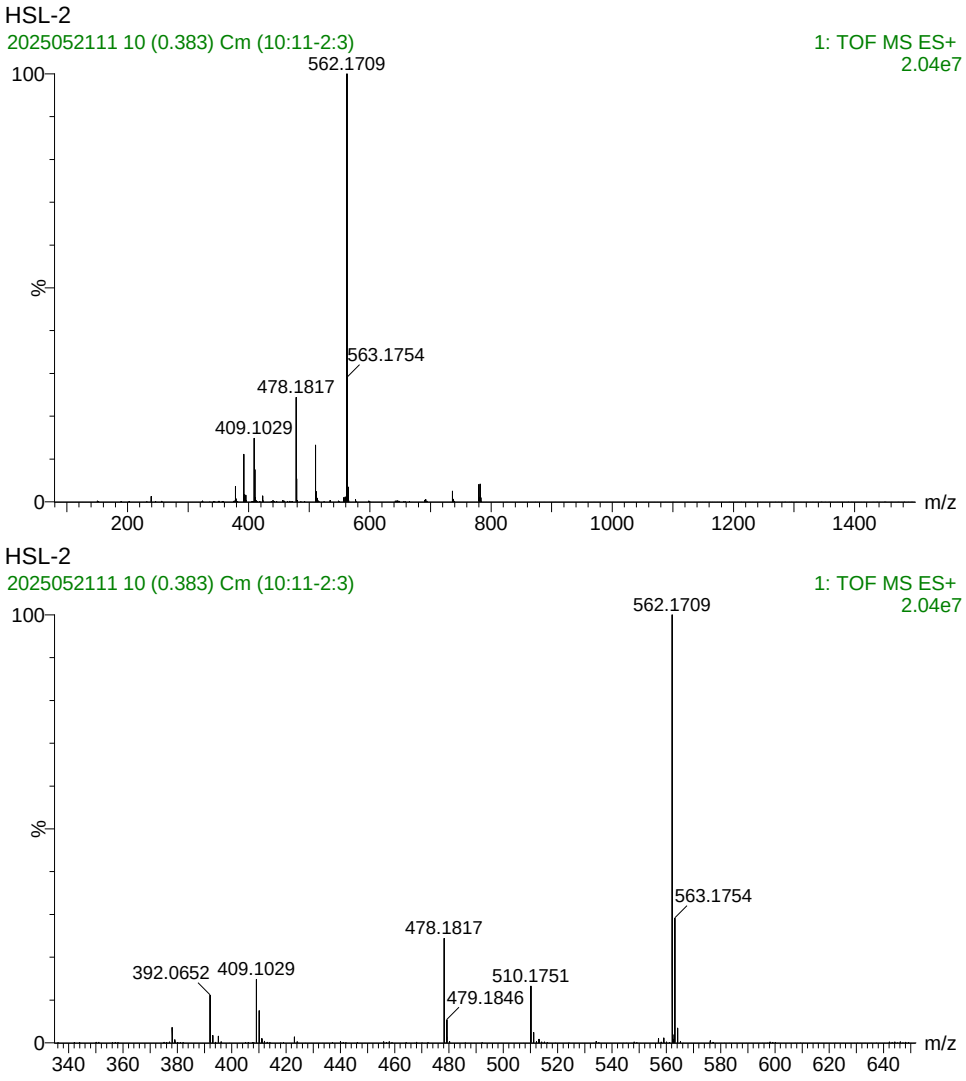

Figure S 10 high resolution mass spectrum of **2p**.

Synthesis of complexes 3p

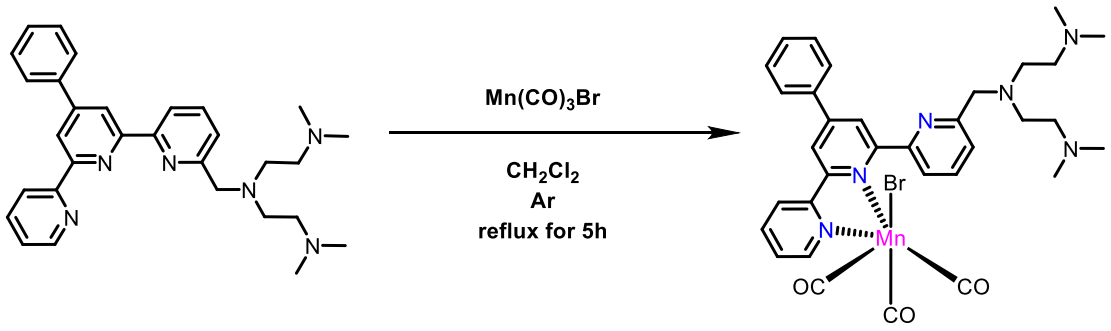

Scheme S 10 preparation of target complex **3p**.

reparation of complexes **3p**. Compound $Mn(CO)_5Br$ (0.14 g, 0.50 mmol) was added to a degassed Dichloromethane solution (3 mL) of 1 equiv **R3** (0.24 g, 0.50 mmol). The resulting orange solution was heated to reflux for 5 h under argon, then allowed to cool to room temperature before filtration. The filtrate was collected and concentrated, then washed with Et_2O and dried in vacuo to afford orange product (0.25 g, 0.36 mmol, yield: 73%). The following were observed for the mixture of atropisomers: ^{1}H NMR (600 MHz, DMSO) δ 9.24 (1H, d), 9.01 (1H, s), 8.89 (1H, d), 8.78 (1H, s), 8.50 – 8.41 (1H, m), 8.30 (1H, s), 8.21 – 8.08 (2H, m), 8.02 – 7.89 (2H, m), 7.88 – 7.80 (1H, m), 7.74 (1H, t), 7.63 (3H, d), 3.66 (2H, s), 2.94 – 2.57 (7H, m), 2.44 – 1.85 (11H, m); IR (KBr, Figure S 19) ν_{CO}: 2021 (s), 1930(s), 1914 (s) cm^{-1}; Anal. Calcd for **3p**, $C_{33}H_{36}BrMnN_6O_3$: C, 56.66; H, 5.19; N, 12.01; found: C, 56.72; H, 5.25; N, 11.96; MS (TOF-ES): m/z = 620.2289 /619.2290 $[M - Br^-]^+$, m/z = 536.2468/535.2464 $[M - Br^- - 3CO]^+$.

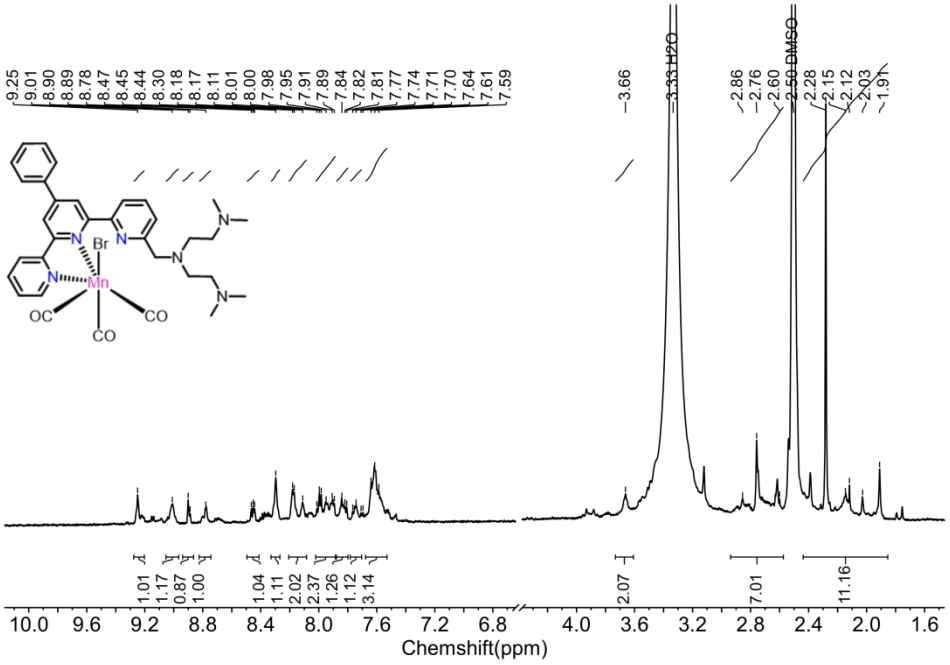

Figure S 1 ^{1}H NMR (DMSO, 600 MHz) spectrum of **3p**.

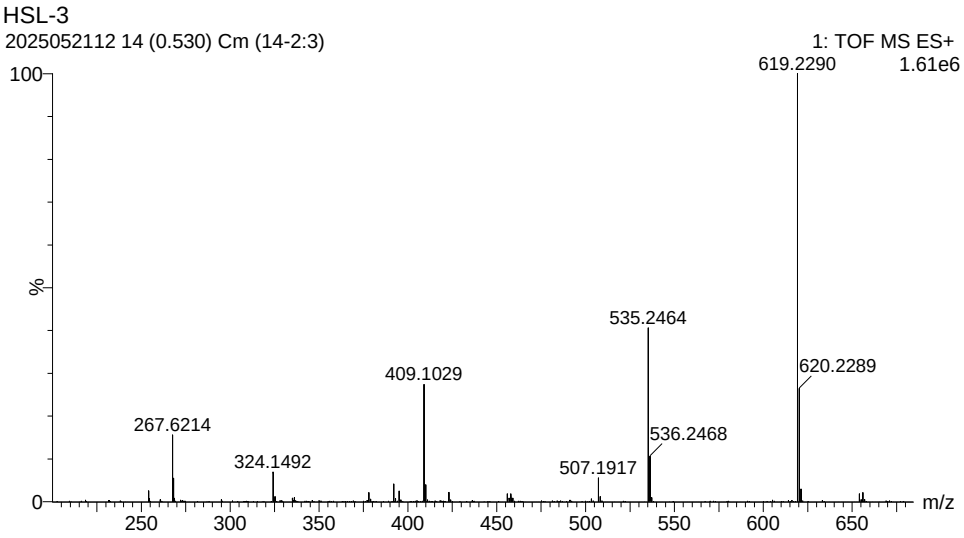

Figure S 2 high resolution mass spectrum of **3p**.

Synthesis of complexes 4p

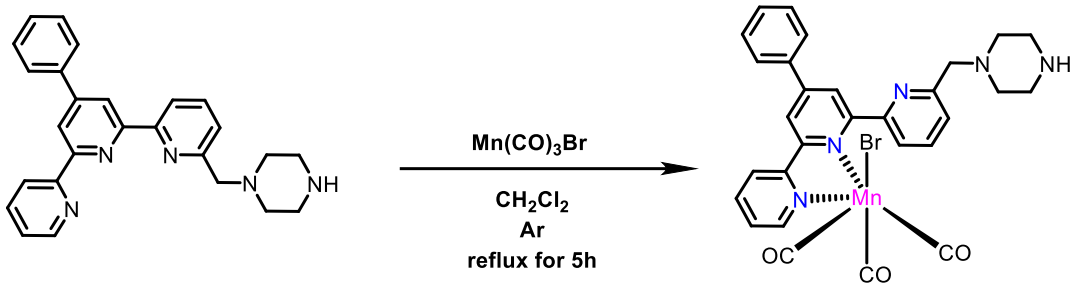

Scheme S 11 preparation of target complex **4p**.

Preparation of complexes **4p**. Compound $Mn(CO)_5Br$ (0.14 g, 0.50 mmol) was added to a degassed Dichloromethane solution (3 mL) of 1 equiv **R4** (0.20 g, 0.50 mmol). The resulting orange solution was heated to reflux for 5 h under argon, then allowed to cool to room temperature before filtration. The filtrate was collected and concentrated, then washed with Et_2O and dried in vacuo to afford orange product (0.28 g, 0.45 mmol, yield: 90%). The following were observed for the mixture of atropisomers: ^{1}H NMR (600 MHz, DMSO) δ 9.23 (1H, dd), 9.14 – 8.93 (2H, m), 8.42 – 7.95(5H,m), 7.93 – 7.84 (1H, m), 7.77 – 7.49 (4H, m), 3.85 – 3.65 (2H, m), 3.08 (3H, m), 2.62 (2H, s); IR (KBr, Figure S 19) *ν*CO: 2021 (s), 1923 (s), 1915 (s) ; Anal. Calcd for **4p**, $C_{29}H_{25}BrMnN_5O_3$: C, 55.61; H, 4.02; N, 11.18; found: C, 55.72; H, 4.11; N, 11.19; MS (TOF-ES): m/z = 546.1331/547.1379 $[M - Br^-]^+$, m/z = 462.1490/463.1516 $[M - Br^- - 3CO]^+$, m/z = 494.1387/495.1414 $[M - Br^- - 3CO + O_2]^+$

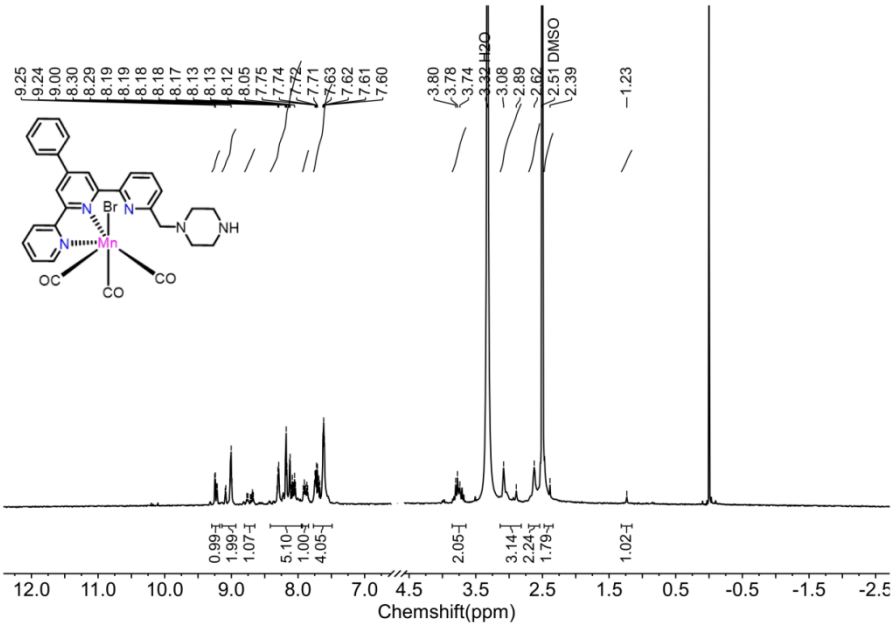

Figure S 13 ^{1}H NMR (DMSO, 600 MHz) spectrum of **4p.**

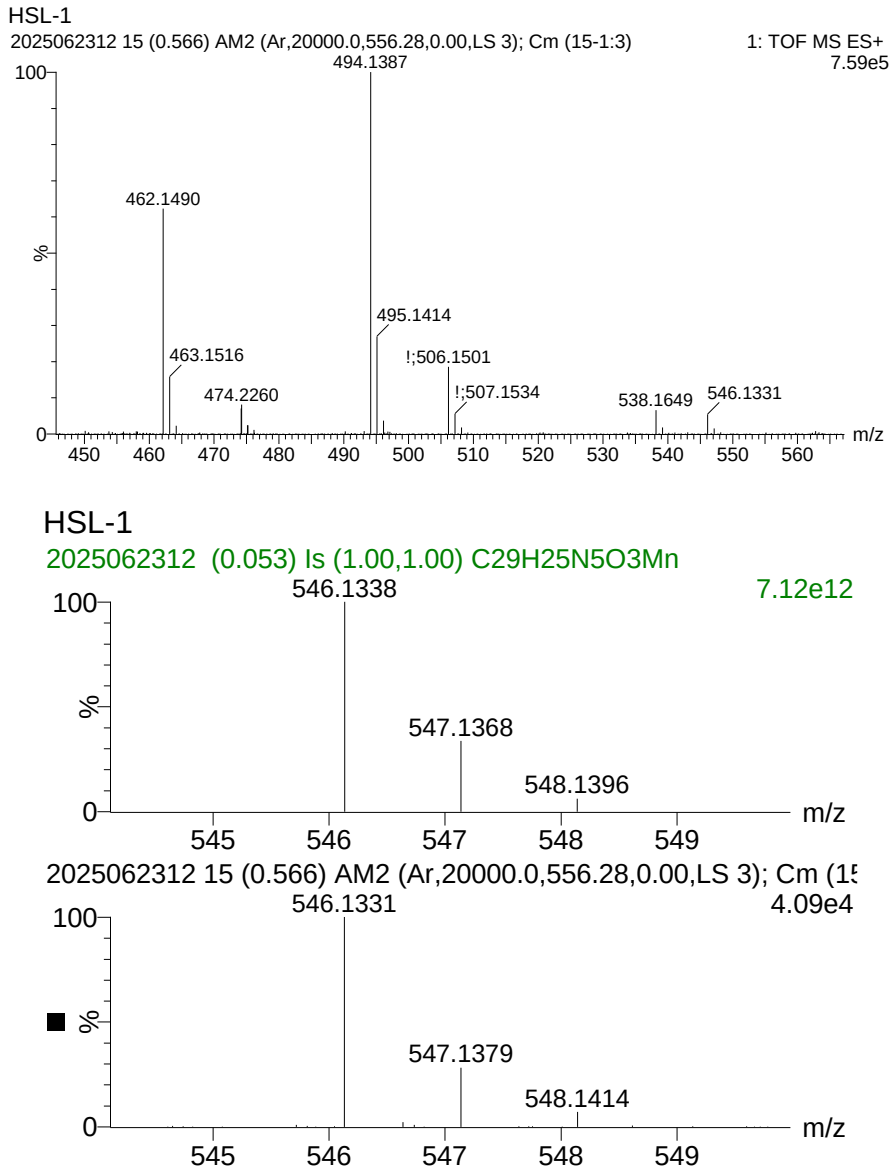

Figure S 14 high resolution mass spectrum of **4p**.

Synthesis of complexes 5p

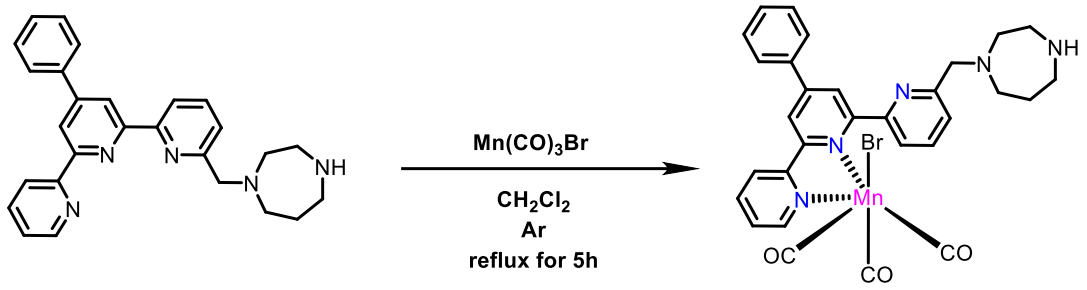

Scheme S 12 preparation of target complex **5p**.

Preparation of complexes **5p**. Compound $Mn(CO)_5Br$ (0.20 g, 0.72 mmol) was added to a degassed Dichloromethane solution (5 mL) of 1 equiv **R5** (0.30 g, 0.72 mmol). The resulting orange solution was heated to reflux for 5 h under argon, then allowed to cool to room temperature before filtration. The filtrate was collected and concentrated, then washed with Et_2O and dried in vacuo to afford orange product (0.40 g, 0.62 mmol, yield: 87%). The following were observed for the mixture of atropisomers: ^{1}H NMR (600 MHz, DMSO) δ 9.23 (1H, dt), 9.13 – 8.96 (2H, m), 8.79 – 8.65 (1H, m), 8.29 (2H, q), 8.21 – 8.07 (3H, m), 7.88 (1H, t), 7.76 (2H, dt), 7.62 (3H, q), 4.01 – 3.81 (2H, m), 3.15 (3H, d), 2.98 – 2.59 (5H,m), 1.88 (2H, s); IR (KBr, Figure S 19) ν_{CO}: 2023 (s), 1933 (s), 1920 (s) cm^{-1}; Anal. Calcd for **5p**, $C_{30}H_{27}BrMnN_5O_3$: C, 56.26; H, 4.25; 8.58; N, 10.94; found: C, 56.35; H, 4.18; N, 10.98; MS (TOF-ES): m/z = 640.0866 / 642.0763 $[M + H]^+$, m/z = 560.1542 $[M - Br^-]^+$.

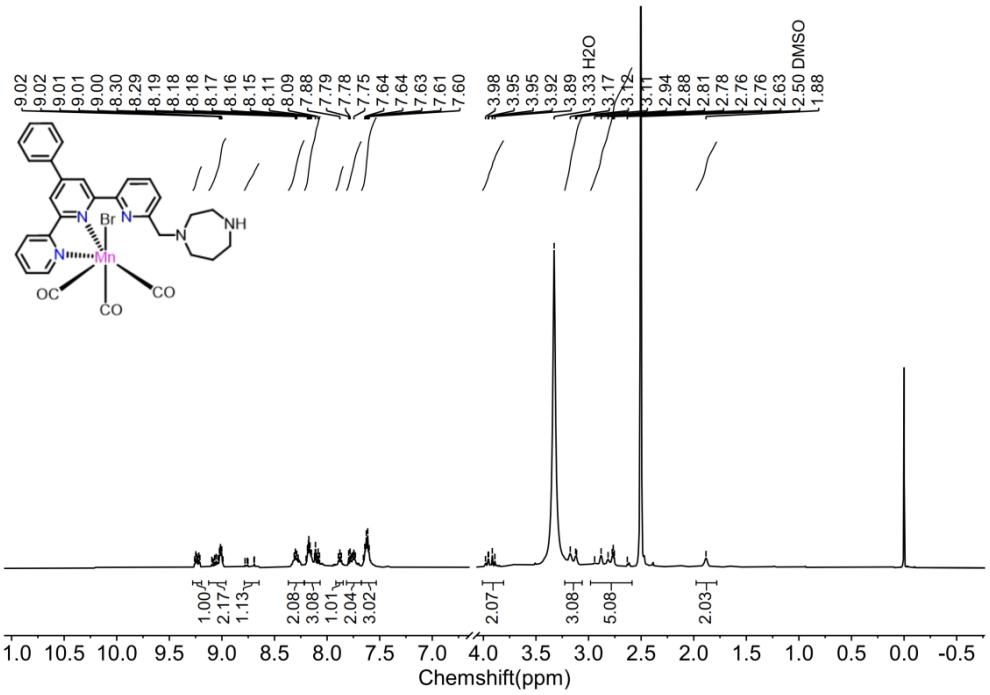

Figure S 15 ^{1}H NMR (DMSO, 600 MHz) spectrum of **5p**.

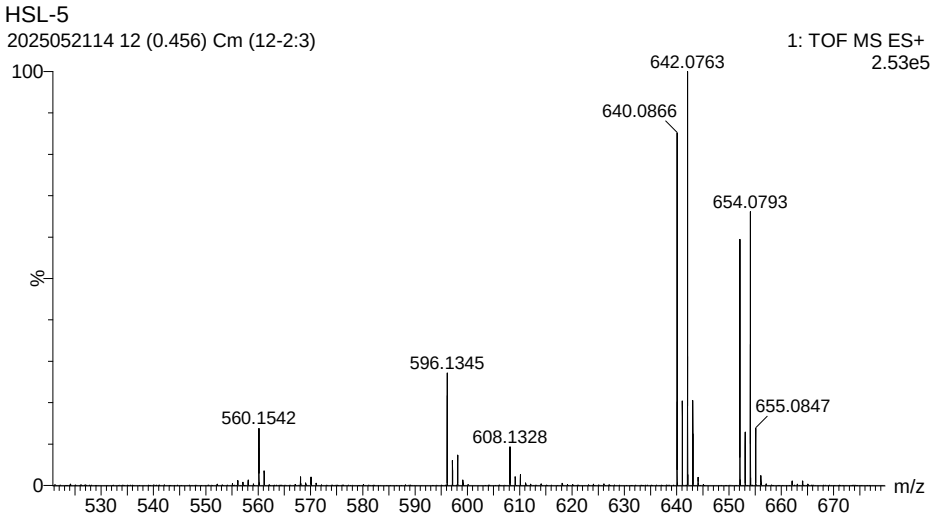

Figure S 13 high resolution mass spectrum of **5p**.

Synthesis of complexes 6p

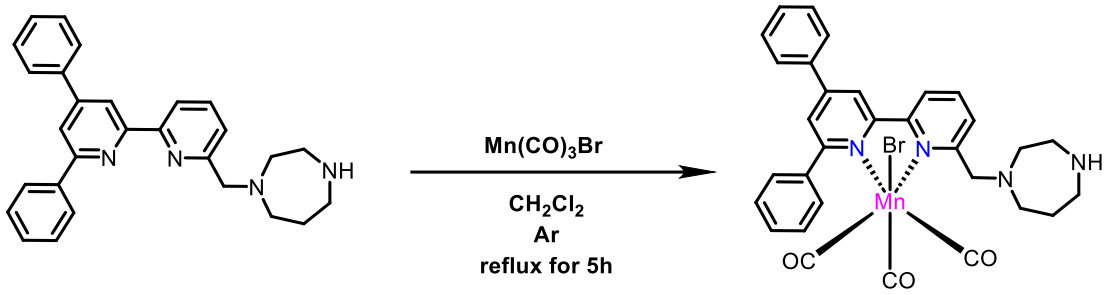

Scheme S 13 preparation of target complex **6p**.

Preparation of complexes **6p**. Compound $Mn(CO)_5Br$ (0.14 g, 0.50 mmol) was added to a degassed Dichloromethane solution (5 mL) of 1 equiv **R6** (0.21 g, 0.50 mmol). The resulting orange solution was heated to reflux for 5 h under argon, then allowed to cool to room temperature before filtration. The filtrate was collected and concentrated, then washed with Et_2O and dried in vacuo to afford orange product (0.26 g, 0.40 mmol, yield: 80%). The following were observed for the mixture of atropisomers: ^{1}H NMR (600 MHz, DMSO) δ 8.94 – 8.84 (1H, m), 8.62 – 8.49 (2H, m), 8.36 (1H, d), 8.30 (1H, s), 8.18 (1H, s), 8.12 – 7.99 (2H, m), 7.97 (1H, d), 7.68 – 7.44 (6H, m), 3.98 (2H, s), 3.19 (4H, d), 3.02 – 2.70 (5H, m), 1.92 (2H, s); IR (KBr, Figure S 19) ν_{CO}: 2018 (s), 1931 (s), 1901 (s) cm^{-1}; Anal. Calcd for **6p**, $C_{31}H_{28}BrMnN_4O_3$: C, 58.23; H, 4.41; N, 8.76; found: C, 58.13; H, 4.37; N, 8.88; MS (TOF-ES): m/z = 559.1693 $[M - Br^-]^+$, m/z = 475.1851/477.1913 $[M - Br^- - 3CO]^+$.

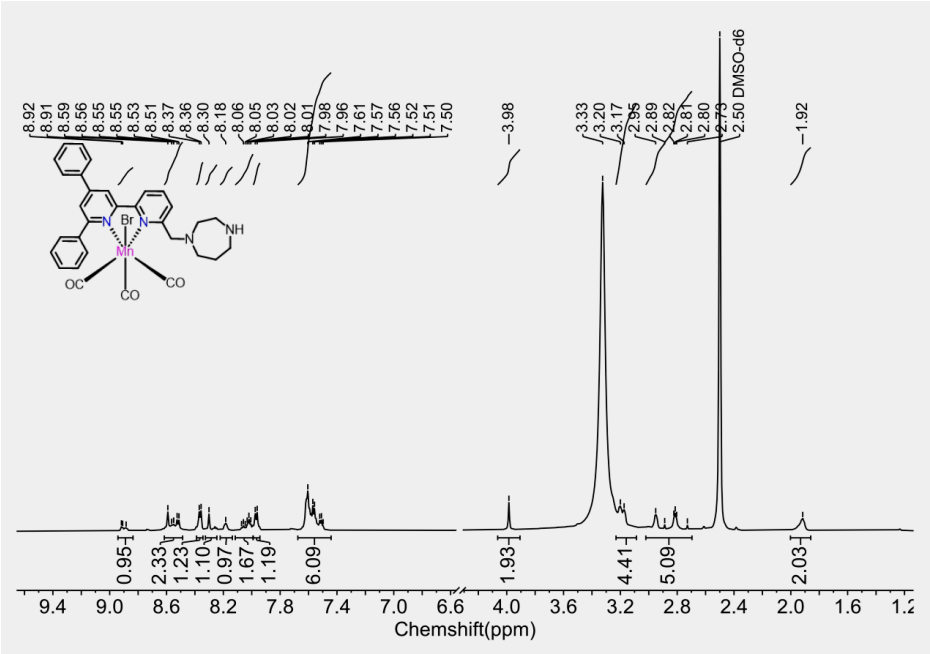

Figure S 17 ^{1}H NMR (DMSO, 600 MHz) spectrum of **6p**.

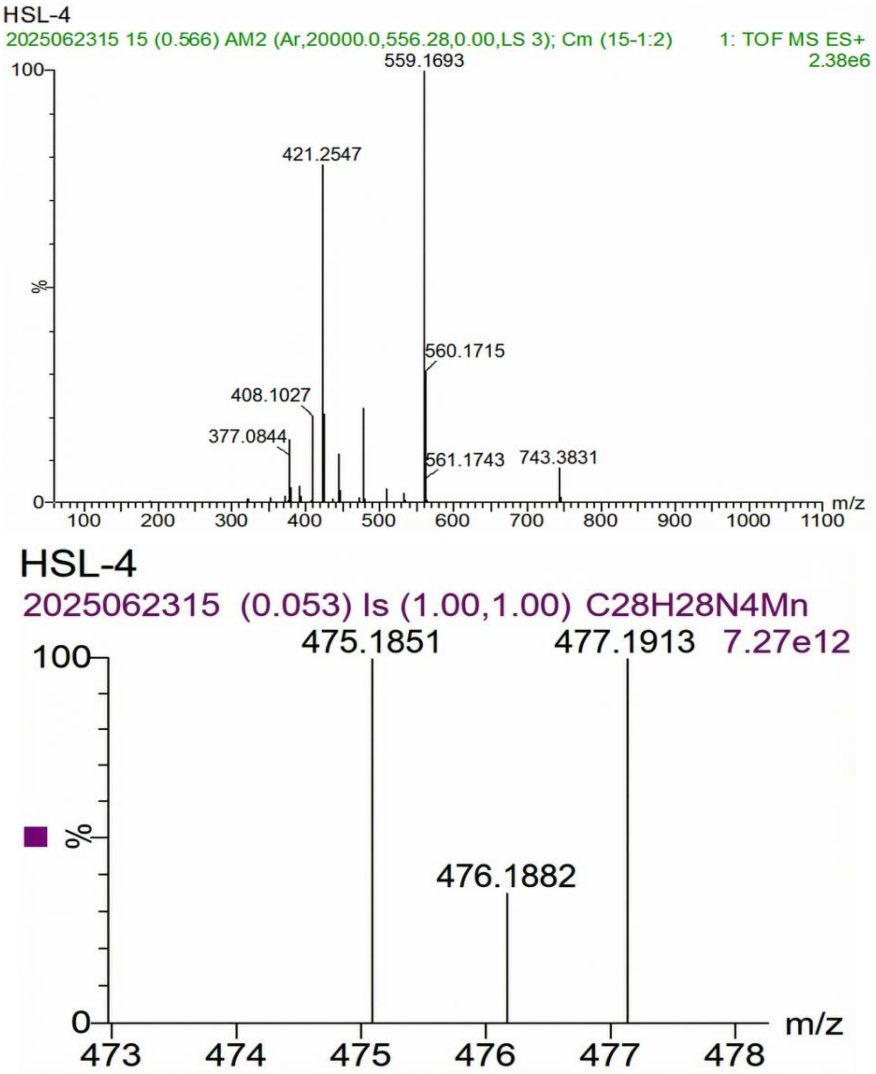

Figure S 18 high resolution mass spectrum of **6p**.

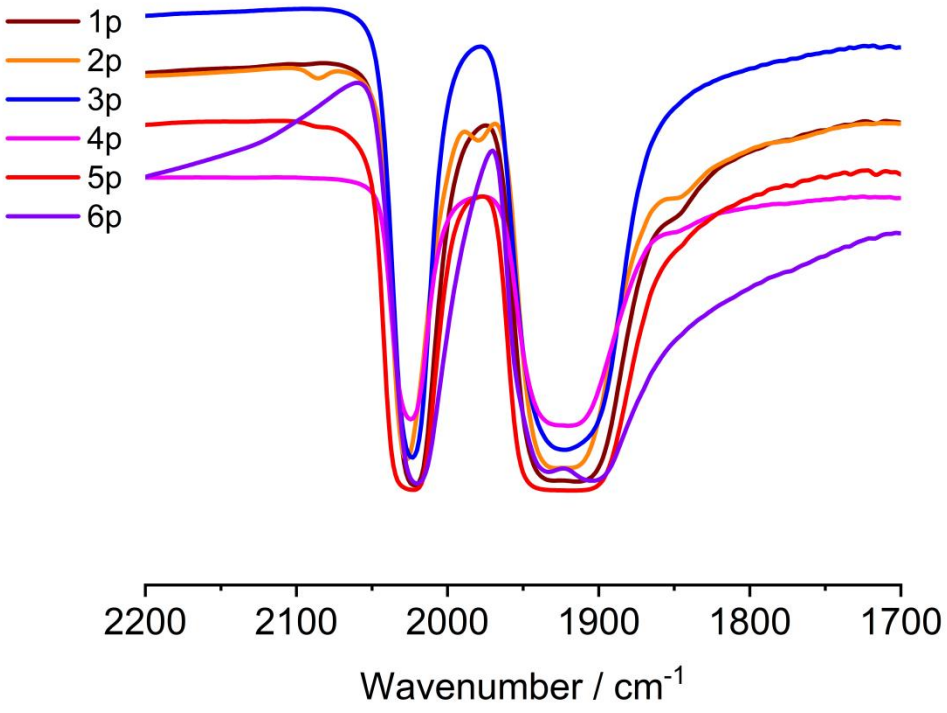

Figure S 19 Experimental FTIR spectra of **1p - 6p** recorded in KBr displaying characteristic ν_{CO} stretching modes for their facial tricarbonyl geometries.

9. Detail discussions on the IR-SEC of complexes

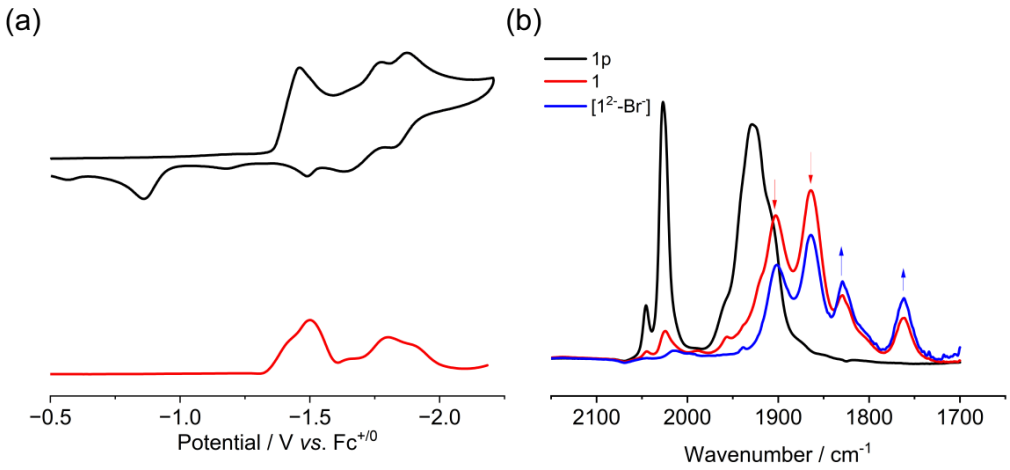

Figure S 20 (a) CV and DPV of complex **1p** (0.5 mM) in acetonitrile under Ar. (b) IR-SEC of 5 mM **1p** under an atmosphere of Ar. The precursor **1p** with $\boldsymbol{k^2 - tpy}$ coordination model (black line). Upon initial electrolysis at -1.35 V, the target complex 1 with $\boldsymbol{k^3 - tpy}$ coordination model (red line, 1903 and 1865 cm^{-1}). The doubly reduced species **[1^{2-} - Br^-]** (blue, 1829 and 1760 cm^{-1}). Glassy carbon working electrode, Ag^+/Ag reference electrode, and Pt wire counter electrode.

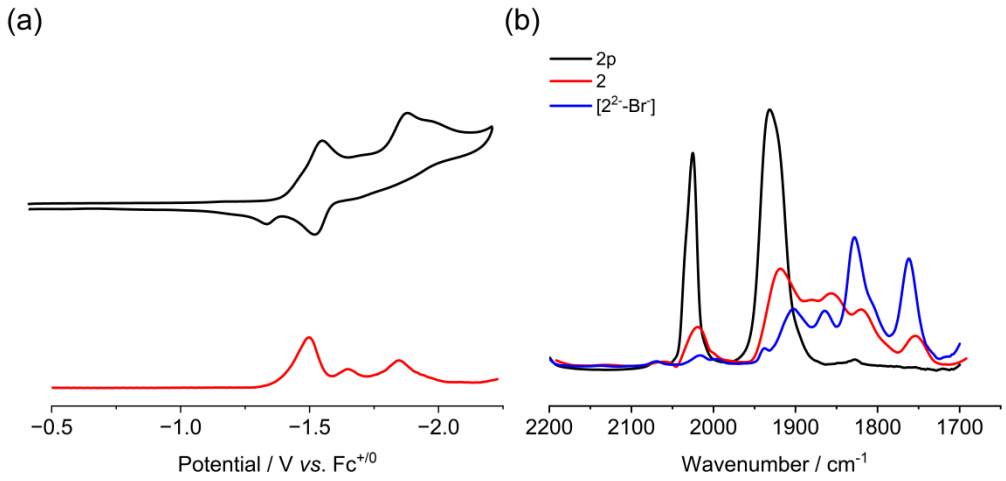

Figure S 21 (a) CV and DPV of complex **2p** (0.5 mM) in acetonitrile under Ar. (b) IR-SEC of 3 mM **2p** under an atmosphere of Ar. The precursor **2p** with $\boldsymbol{k^2 - tpy}$ coordination model (black line). Upon initial electrolysis at -1.2 V, the target complex **2** with $\boldsymbol{k^3 - tpy}$ coordination model (red line, 1910 and 1854 cm^{-1}), the doubly reduced species **[2^{2-} - Br^-]** (blue, 1827 and 1762 cm^{-1}). Glassy carbon working electrode, Ag^+/Ag reference electrode, and Pt wire counter electrode.

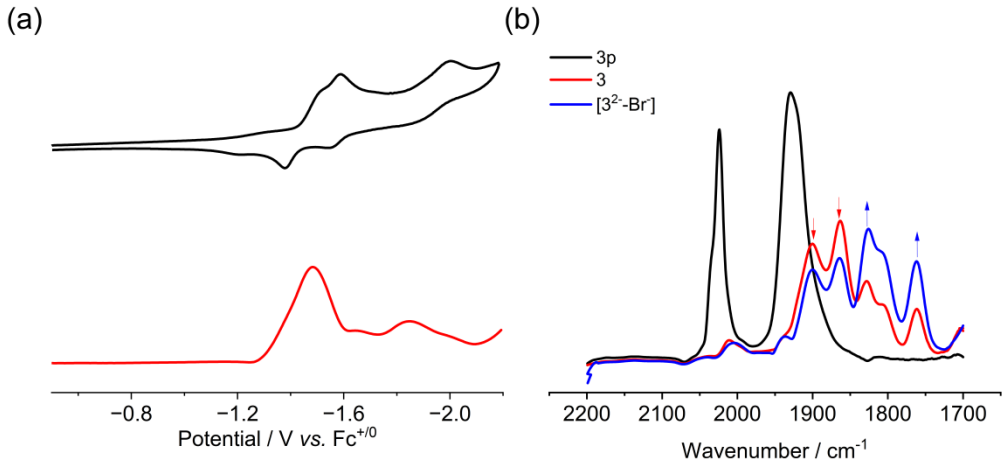

Figure S 22 (a) CV and DPV of complex **3p** (0.5 mM) in acetonitrile under Ar. (b) IR-SEC of 3mM **3p** under an atmosphere of Ar. The precursor **3p** with $\boldsymbol{k^2 - tpy}$ coordination model (black line). Upon initial electrolysis at -1.24 V, the target complex **3** with $\boldsymbol{k^3 - tpy}$ coordination model (red line, 1900 and 1854 cm^{-1}). The doubly reduced species **[3^{2-} - Br^-]** (blue, 1826 and 1761 cm^{-1}). Glassy carbon working electrode, Ag^+/Ag reference electrode, and Pt wire counter electrode.

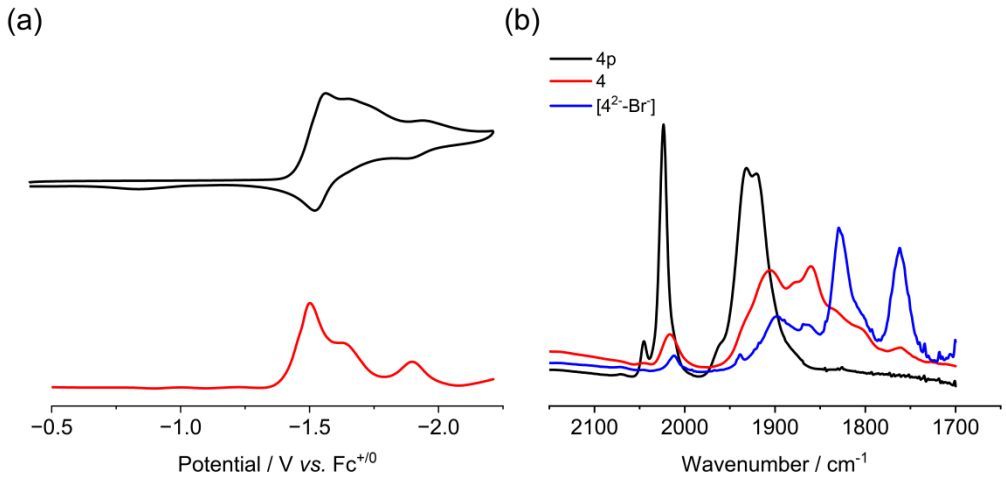

Figure S 23 (a) CV and DPV of complex **4p** (0.5 mM) in acetonitrile under Ar. (b) IR-SEC of 5 mM **4p** under an atmosphere of Ar. The precursor **4p** with $\boldsymbol{k^2 - tpy}$ coordination model (black line). Upon initial electrolysis at -1.2 V, the target complex **4** with $\boldsymbol{k^3 - tpy}$ coordination model (red line, 1903 and 1860 cm^{-1}). The doubly reduced species **[4^{2-} - Br^{-}]** (blue, 1827 and 1761 cm^{-1}). Glassy carbon working electrode, Ag^{+}/Ag reference electrode, and Pt wire counter electrode.

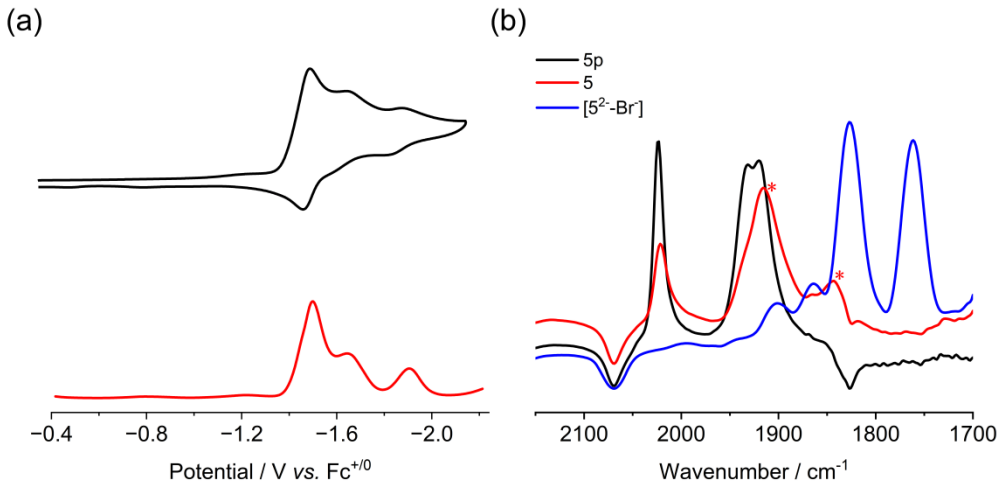

Figure S 24 (a) CV and DPV of complex **5p** (0.5 mM) in acetonitrile under Ar. (b) IR-SEC of 3 mM **5p** under an atmosphere of Ar. The precursor **5p** with $\boldsymbol{k^2 - tpy}$ coordination model (black line). Upon initial electrolysis at -1.21 V, the target complex 5 with $\boldsymbol{k^3 - tpy}$ coordination model (red line). The doubly reduced species **[5^{2-} - Br^-]** (blue, 1827 and 1762 cm^{-1}). Glassy carbon working electrode, Ag^+/Ag reference electrode, and Pt wire counter electrode.

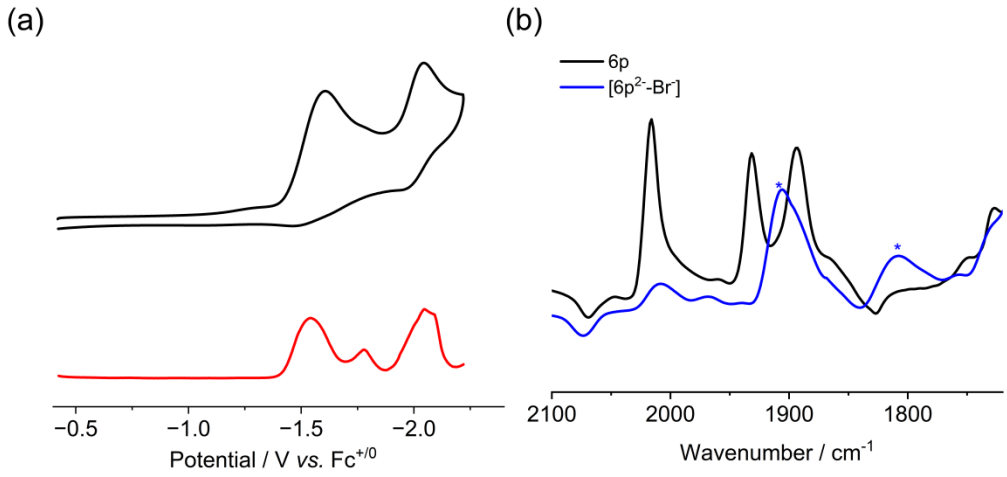

Figure S 25 (a) CV and DPV of complex **6p** (0.5 mM) in acetonitrile under Ar. (b) IR-SEC of 3 mM **6p** under an atmosphere of Ar. The precursor **6p** with $\boldsymbol{k^2 - bpy}$ coordination model (black line). The doubly reduced species **[6p^{2-} - Br$^-$]** (blue, 1903 and 1806 cm^{-1}). Glassy carbon working electrode, Ag$^+$/Ag reference electrode, and Pt wire counter electrode.

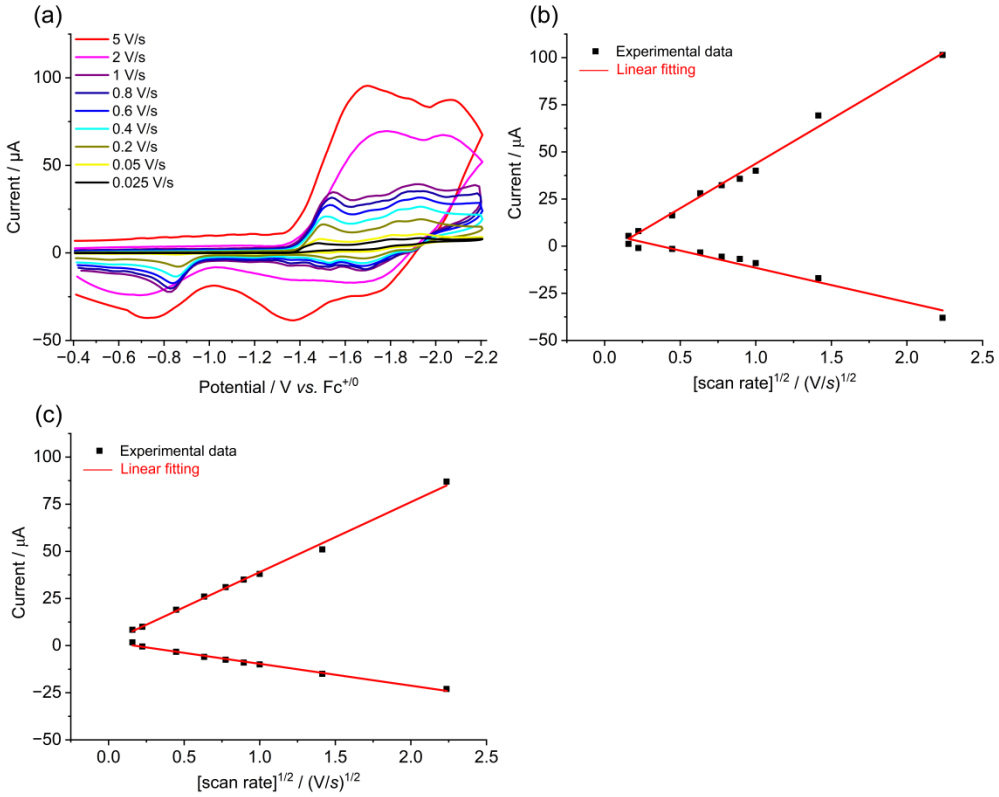

Figure S 26 (a) CV of complex **1p** (0.5 mM) with scan rate (v) varied from 0.025 V/s to 5 V/s under Ar; (b) Plot of redox peak current (i_p) *vs.* $v^{1/2}$ for complex **1p** at -1.49V； (c) Plot of redox peak current (i_p) *vs.* $v^{1/2}$ for complex **1p** at -1.94V. Voltammograms are taken with 0.1 M $^{n}Bu_4NPF_6$ in MeCN solution. Glassy carbon working electrode, Ag^+/Ag reference electrode, and Pt wire counter electrode

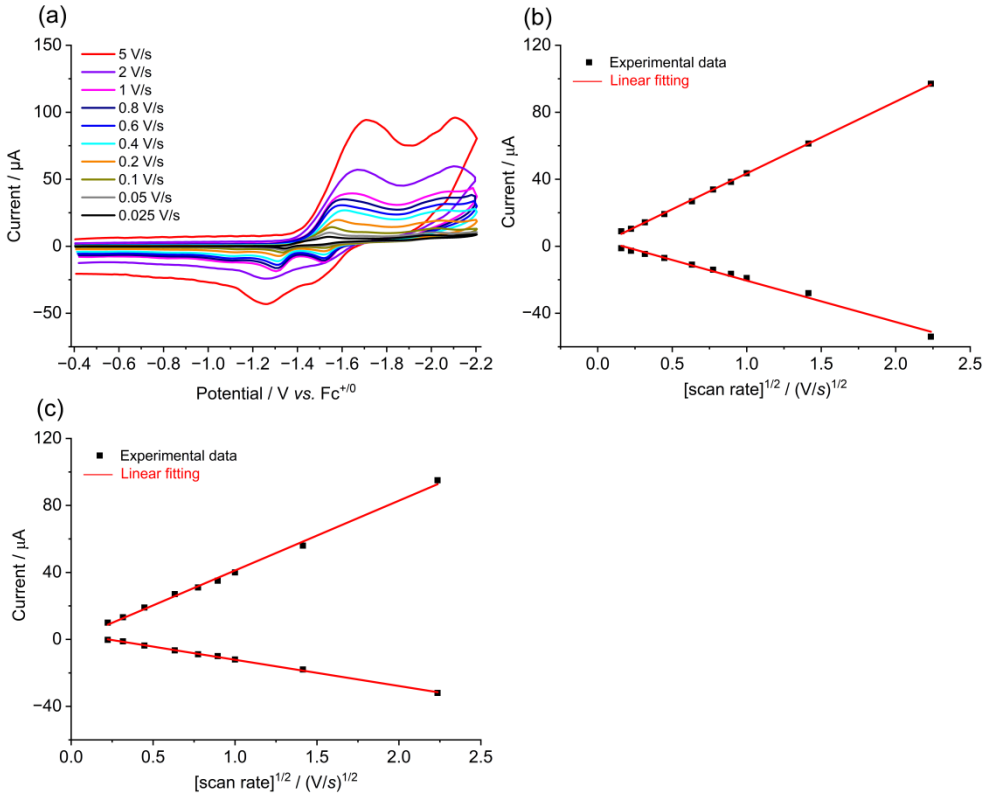

Figure S 27 (a) CV of complex **2p** (0.5 mM) with scan rate (v) varied from 0.025 V/s to 5 V/s under Ar; (b) Plot of redox peak current (i_p) *vs.* $v^{1/2}$ for complex **2p** at -1.53V； (c) Plot of redox peak current (i_p) *vs.* $v^{1/2}$ for complex **2p** at -1.88V. Voltammograms are taken with 0.1 M nBu_4NPF_6 in MeCN solution. Glassy carbon working electrode, Ag^+/Ag reference electrode, and Pt wire counter electrode

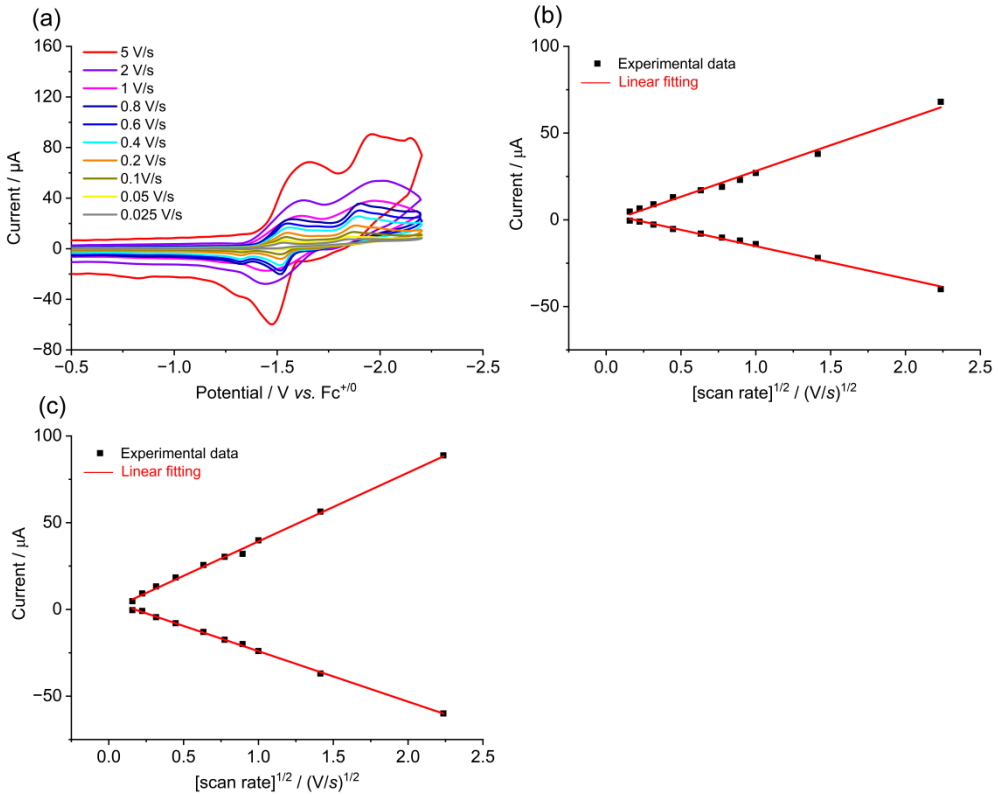

Figure S 28 (a) CV of complex **3p** (0.5 mM) with scan rate (v) varied from 0.025 V/s to 5 V/s under Ar; (b) Plot of redox peak current (i_p) *vs.* $v^{1/2}$ for complex **3p** at -1.53V; (c) Plot of redox peak current (i_p) *vs.* $v^{1/2}$ for complex **3p** at -1.96V. Voltammograms are taken with 0.1 M nBu_4NPF_6 in MeCN solution. Glassy carbon working electrode, Ag^+/Ag reference electrode, and Pt wire counter

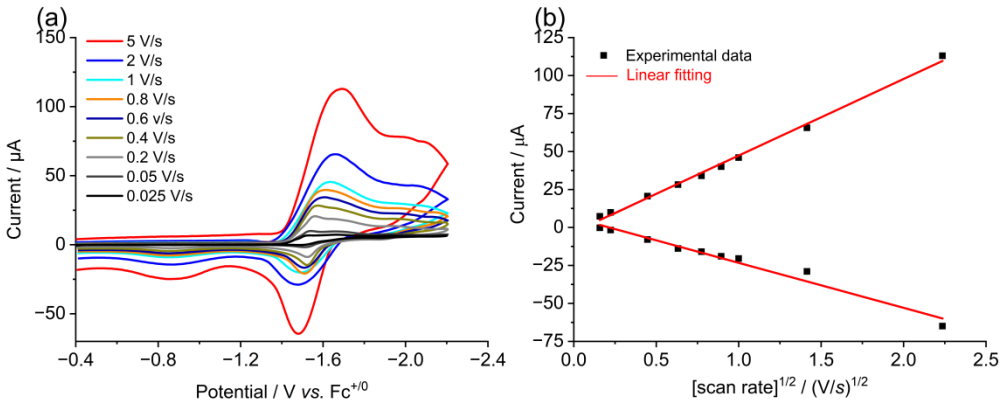

Figure S 29 (a) CV of complex **4p** (0.5 mM) with scan rate (v) varied from 0.025 V/s to 5 V/s under Ar; (b) Plot of redox peak current (i_p) *vs.* $v^{1/2}$ for complex **4p**. Voltammograms are taken with 0.1 M nBu_4NPF_6 in MeCN solution. Glassy carbon working electrode, Ag^+/Ag reference electrode, and Pt wire counter electrode.

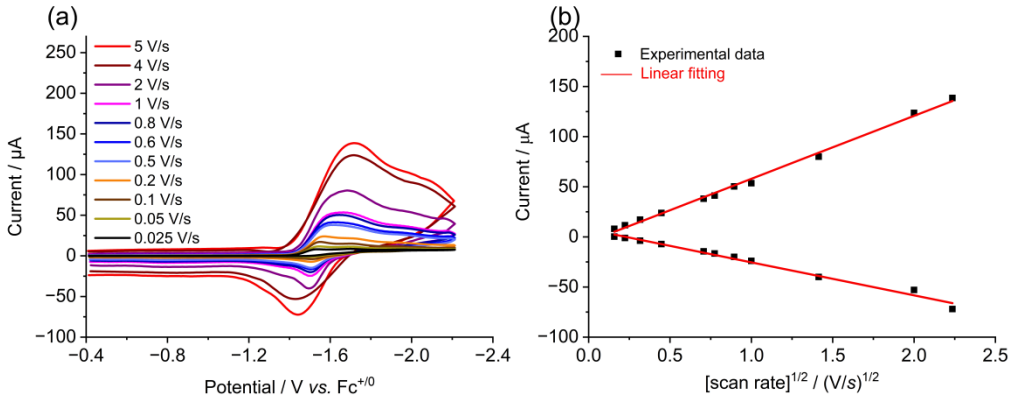

Figure S 30 CV of complex **5p** (0.5 mM) with scan rate (v) varied from 0.025 V/s to 5 V/s under Ar; (b) Plot of redox peak current (i_p) *vs.* $v^{1/2}$ for complex **5p**. Voltammograms are taken with 0.1 M nBu_4NPF_6 in MeCN solution. Glassy carbon working electrode, Ag^+/Ag reference electrode, and Pt wire counter electrode.

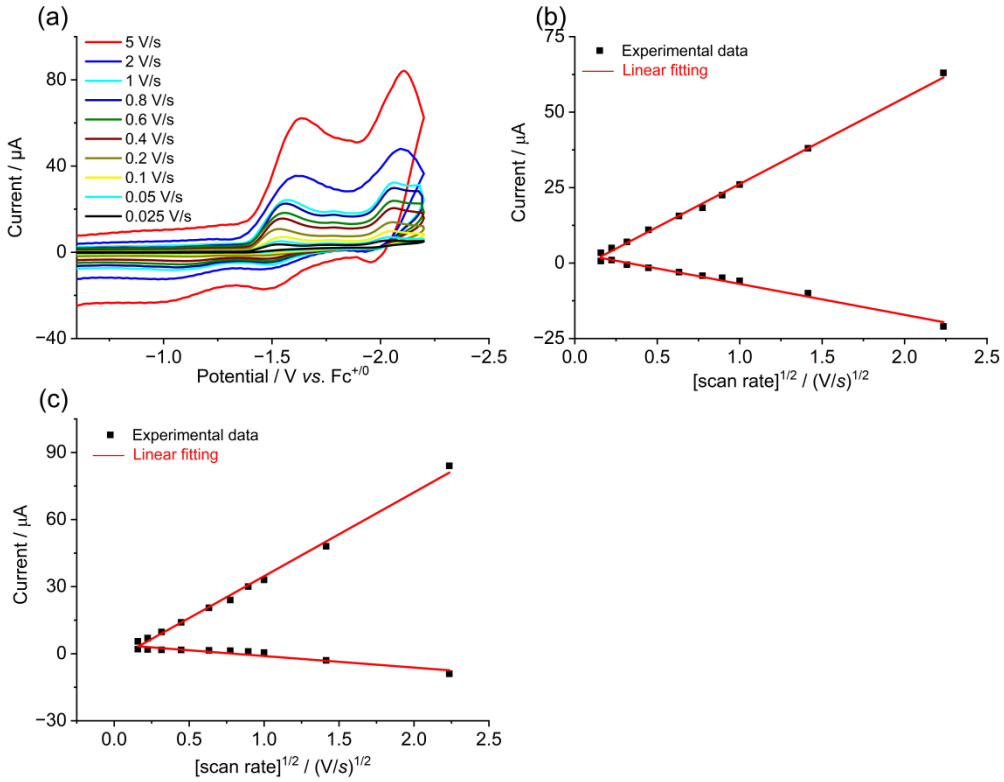

Figure S 31 (a) CV of complex **6p** (0.5 mM) with scan rate (v) varied from 0.025 V/s to 5 V/s under Ar; (b) Plot of redox peak current (i_p) *vs.* $v^{1/2}$ for complex **6p** at -1.53V; (c) Plot of redox peak current (i_p) *vs.* $v^{1/2}$ for complex **6p** at -2.15V. Voltammograms are taken with 0.1 M nBu_4NPF_6 in MeCN solution. Glassy carbon working electrode, Ag^+/Ag reference electrode, and Pt wire counter

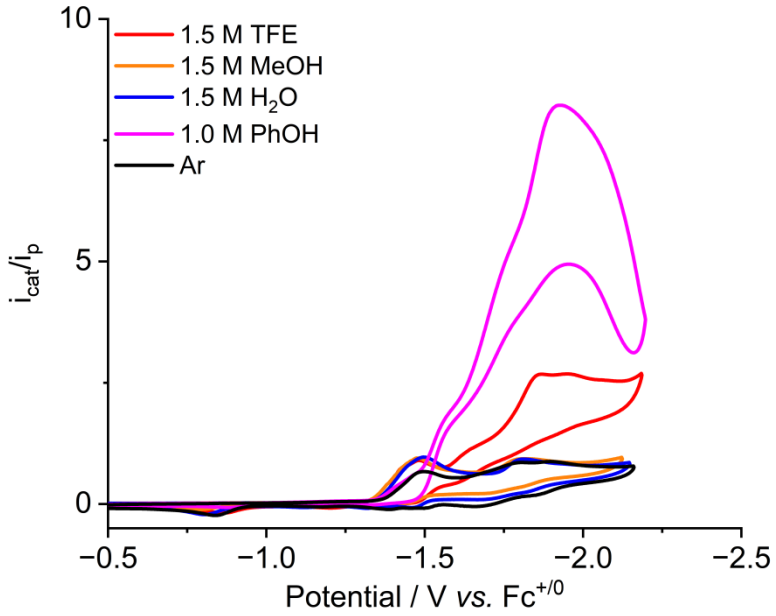

Figure S 32 CV of 0.5 mM **1p** with different proton sources under Ar. Voltammograms are taken at a scan rate of 100 mV/s with 0.1 M $^{n}Bu_4NPF_6$ in MeCN solution. Glassy carbon working electrode, Ag^{+}/Ag reference electrode, and Pt wire counter electrode.

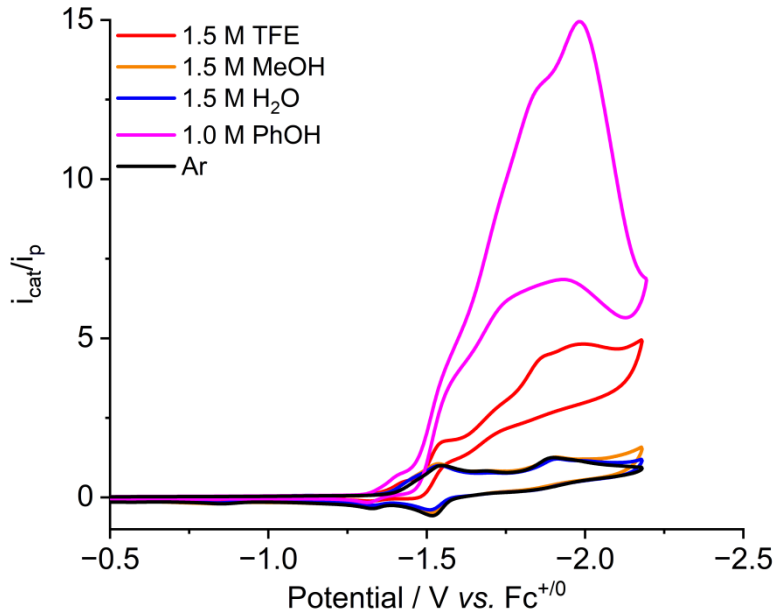

Figure S 33 CV of 0.5 mM **2p** with different proton sources under Ar. Voltammograms are taken at a scan rate of 100 mV/s with 0.1 M $^{n}Bu_4NPF_6$ in MeCN solution. Glassy carbon working electrode, Ag^{+}/Ag reference electrode, and Pt wire counter electrode.

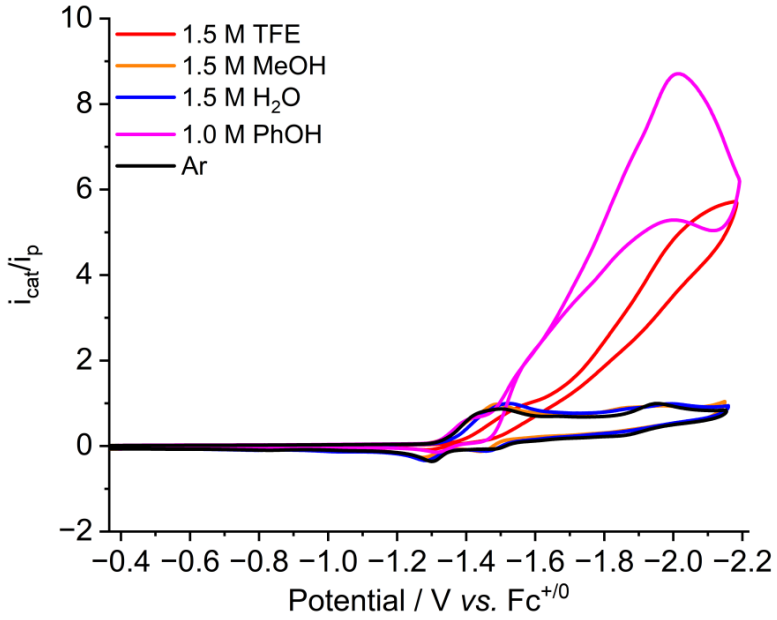

Figure S 34 CV of 0.5 mM **3p** with different proton sources under Ar. Voltammograms are taken at a scan rate of 100 mV/s with 0.1 M $^{n}Bu_4NPF_6$ in MeCN solution. Glassy carbon working electrode, Ag^{+}/Ag reference electrode, and Pt wire counter electrode.

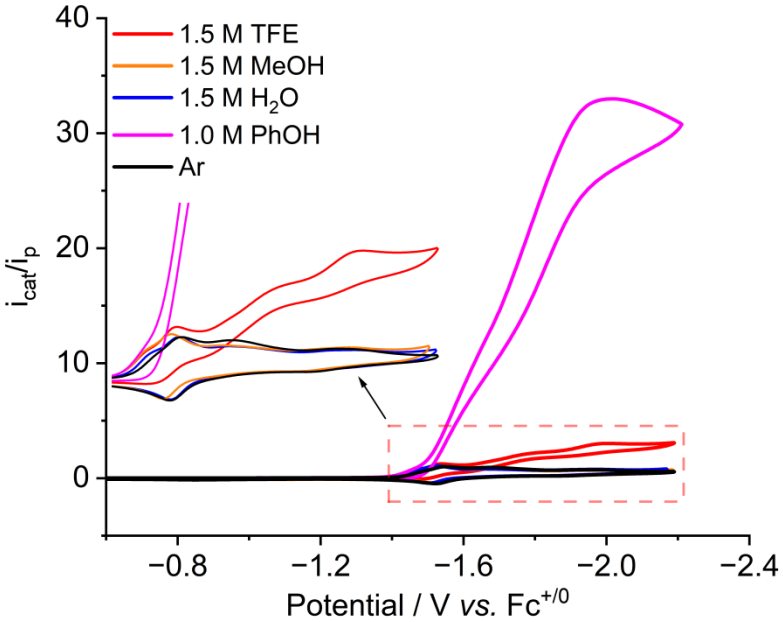

Figure S 35 CV of 0.5 mM **4p** with different proton sources under Ar. Voltammograms are taken at a scan rate of 100 mV/s with 0.1 M $^{n}Bu_4NPF_6$ in MeCN solution. Glassy carbon working electrode, Ag^{+}/Ag reference electrode, and Pt wire counter electrode.

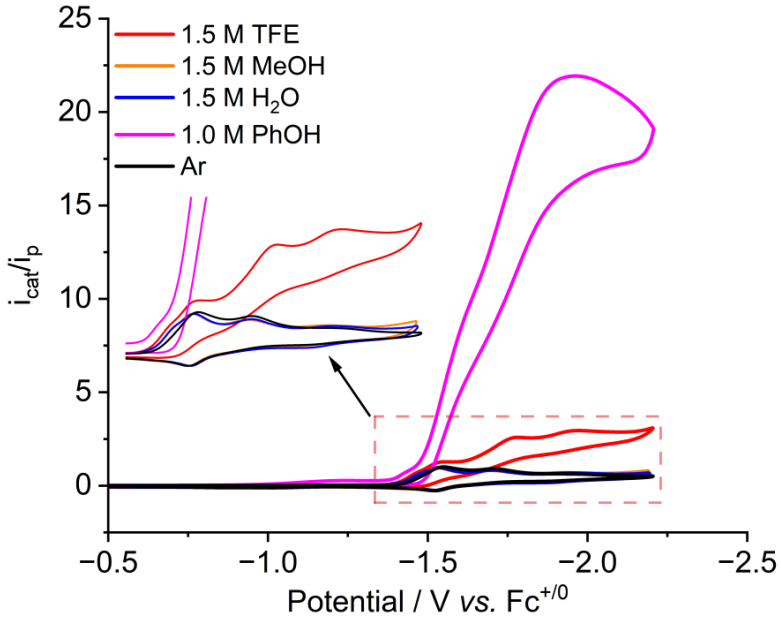

Figure S 36 CV of 0.5 mM **5p** with different proton sources under Ar. Voltammograms are taken at a scan rate of 100 mV/s with 0.1 M $^{n}Bu_4NPF_6$ in MeCN solution. Glassy carbon working electrode, Ag^{+}/Ag reference electrode, and Pt wire counter electrode.

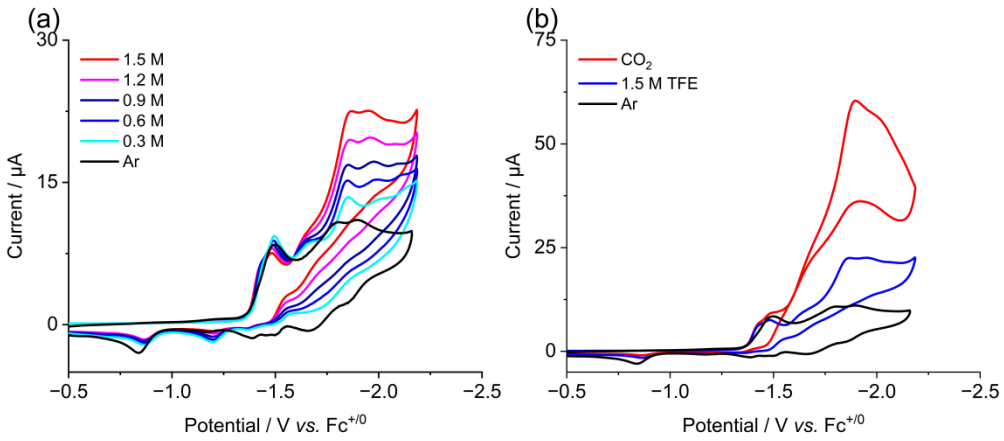

Figure S 37 (a) CVs of 0.5 mM **1p** with varied concentrations of TFE under Ar. (b) CVs show 0.5 mM **1p** with 1.5 M TFE under Ar, and saturated with CO_2 in the presence of 1.5 M TFE. Voltammograms are taken at a scan rate of 100 mV/s with 0.1 M $^{n}Bu_4NPF_6$ in MeCN solution. Glassy carbon working electrode, Ag^+/Ag reference electrode, and Pt wire counter electrode.

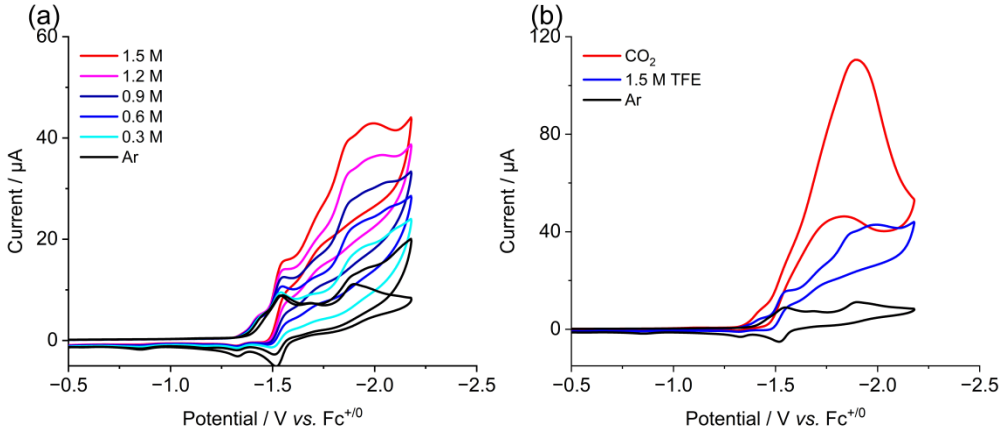

Figure S 38 (a) CVs of 0.5 mM **2p** with varied concentrations of TFE under Ar. (b) CVs show 0.5 mM **2p** with 1.5 M TFE under Ar, and saturated with CO_2 in the presence of 1.5 M TFE Voltammograms are taken at a scan rate of 100 mV/s with 0.1 M $^{n}Bu_4NPF_6$ in MeCN solution. Glassy carbon working electrode, Ag^+/Ag reference electrode, and Pt wire counter electrode.

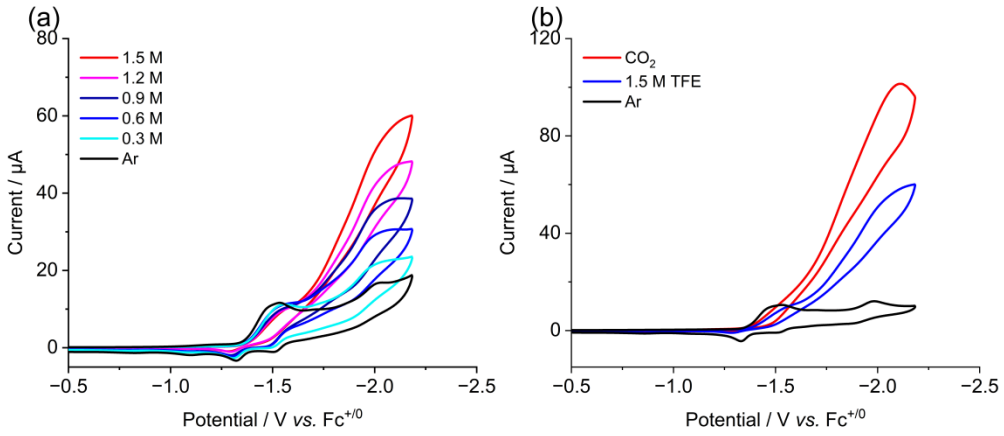

Figure S 39 (a) CVs of 0.5 mM **3p** with varied concentrations of TFE under Ar. (b) CVs show 0.5 mM **3p** with 1.5 M TFE under Ar, and saturated with CO_2 in the presence of 1.5 M TFE. Voltammograms are taken at a scan rate of 100 mV/s with 0.1 M $^{n}Bu_4NPF_6$ in MeCN solution. Glassy carbon working electrode, Ag^{+}/Ag reference electrode, and Pt wire counter electrode.

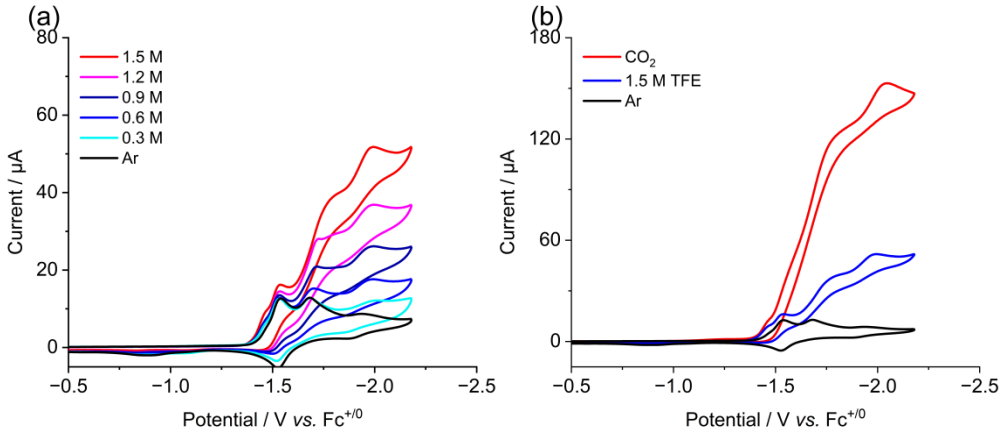

Figure S 40 (a) CVs of 0.5 mM **4p** with varied concentrations of TFE under Ar. (b) CVs show 0.5 mM **4p** with 1.5 M TFE under Ar, and saturated with CO_2 in the presence of 1.5 M TFE. Voltammograms are taken at a scan rate of 100 mV/s with 0.1 M $^{n}Bu_4NPF_6$ in MeCN solution. Glassy carbon working electrode, Ag^{+}/Ag reference electrode, and Pt wire counter electrode.

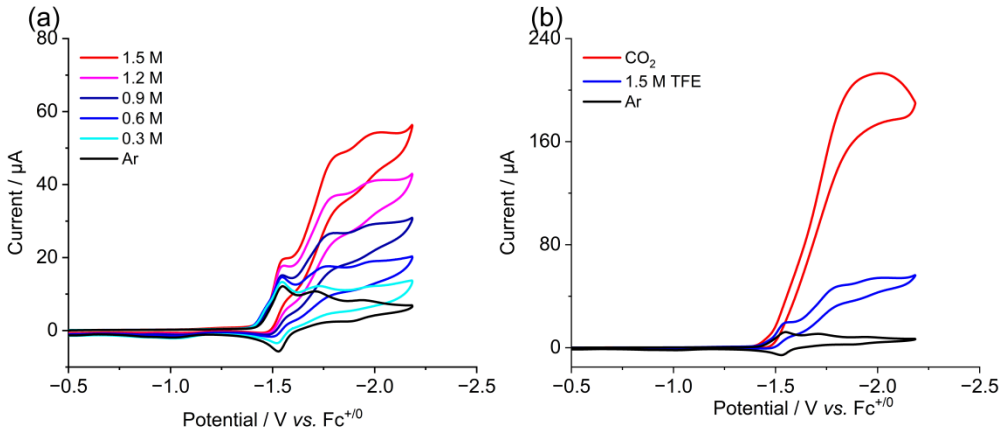

Figure S 41 (a) CVs of 0.5 mM **5p** with varied concentrations of TFE under Ar. (b) CVs show 0.5 mM **5p** with 1.5 M TFE under Ar, and saturated with CO_2 in the presence of 1.5 M TFE. Voltammograms are taken at a scan rate of 100 mV/s with 0.1 M $^{n}Bu_4NPF_6$ in MeCN solution. Glassy carbon working electrode, Ag^+/Ag reference electrode, and Pt wire counter electrode.

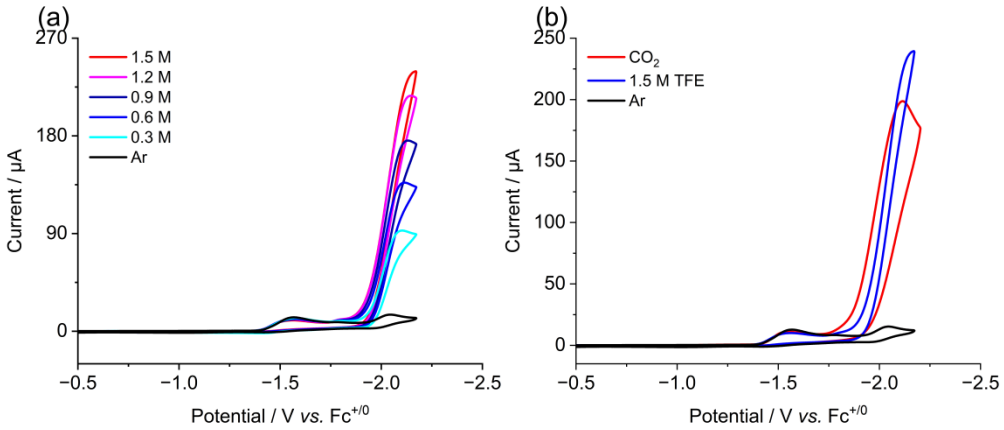

Figure S 42 (a) CVs of 0.5 mM **6p** with varied concentrations of TFE under Ar. (b) CVs show 0.5 mM **6p** with 1.5 M TFE under Ar, and saturated with CO_2 in the presence of 1.5 M TFE. Voltammograms are taken at a scan rate of 100 mV/s with 0.1 M $^{n}Bu_4NPF_6$ in MeCN solution. Glassy carbon working electrode, Ag^+/Ag reference electrode, and Pt wire counter electrode.

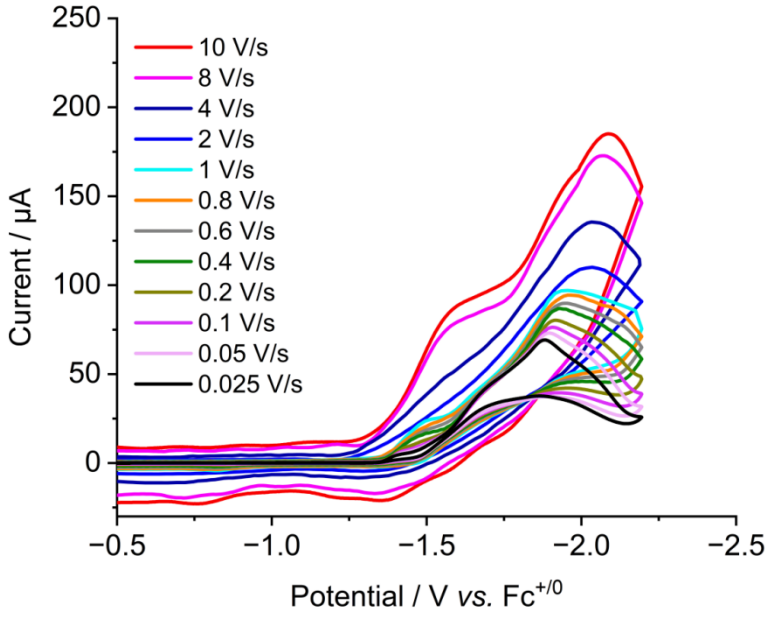

Figure S 43 Cyclic voltammograms of complex **1p** (0.5 mM) with scan rate (v) varied from 0.025 V/s to 10 V/s in the presence of 1.5 M TFE under CO_2. Voltammograms are taken with 0.1 M $^{n}Bu_4NPF_6$ in MeCN solution. Glassy carbon working electrode, Ag^+/Ag reference electrode, and Pt wire counter electrode.

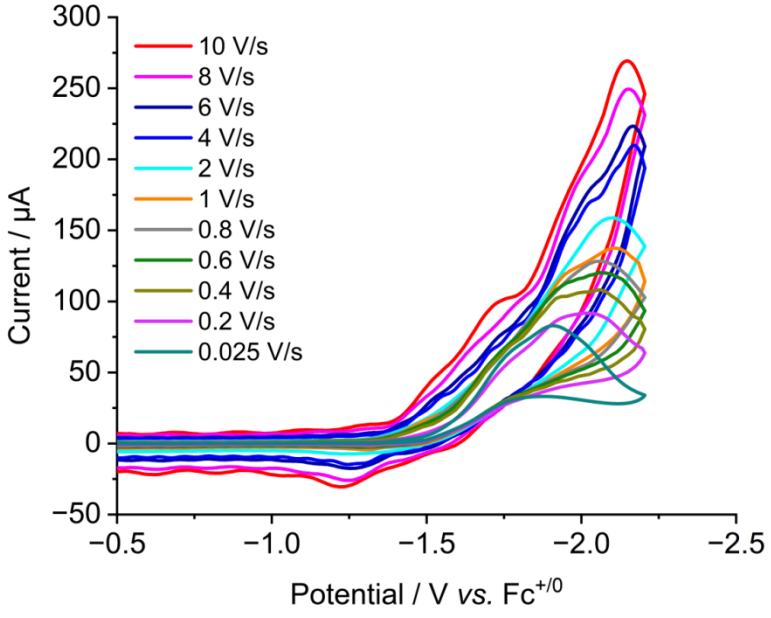

Figure S 44 Cyclic voltammograms of complex **2p** (0.5 mM) with scan rate (v) varied from 0.025 V/s to 10 V/s in the presence of 1.5 M TFE under CO_2. Voltammograms are taken with 0.1 M $^{n}Bu_4NPF_6$ in MeCN solution. Glassy carbon working electrode, Ag^+/Ag reference electrode, and Pt

wire counter electrode.

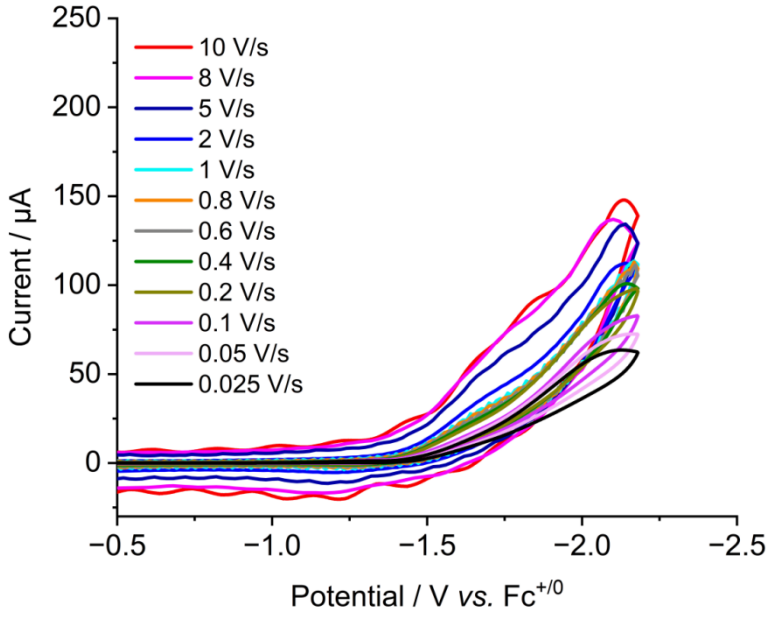

Figure S 45 Cyclic voltammograms of complex **3p** (0.5 mM) with scan rate (v) varied from 0.025 V/s to 10 V/s in the presence of 1.5 M TFE under CO_2. Voltammograms are taken with 0.1 M $^{n}Bu_4NPF_6$ in MeCN solution. Glassy carbon working electrode, Ag^+/Ag reference electrode, and Pt wire counter electrode.

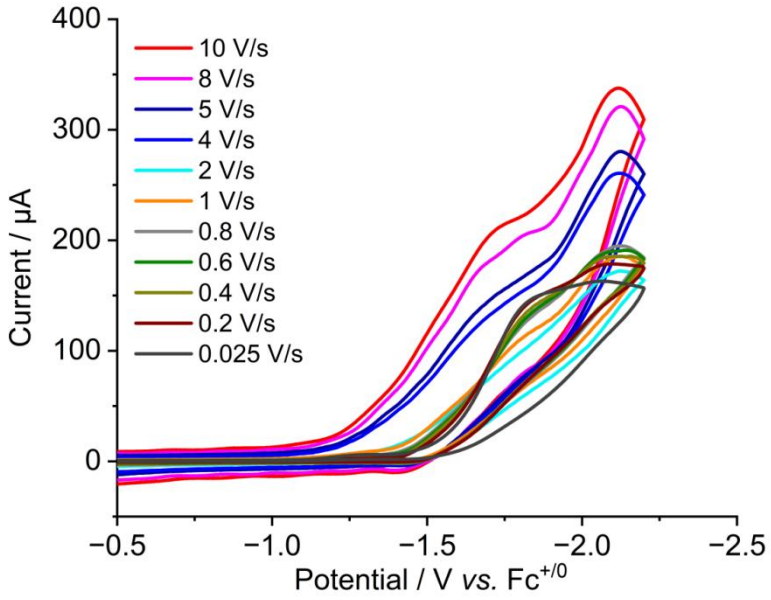

Figure S 46 Cyclic voltammograms of complex **4p** (0.5 mM) with scan rate (v) varied from 0.025 V/s to 10 V/s in the presence of 1.5 M TFE under CO_2. Voltammograms are taken with 0.1 M $^{n}Bu_4NPF_6$ in MeCN solution. Glassy carbon working electrode, Ag^+/Ag reference electrode, and Pt

wire counter electrode.

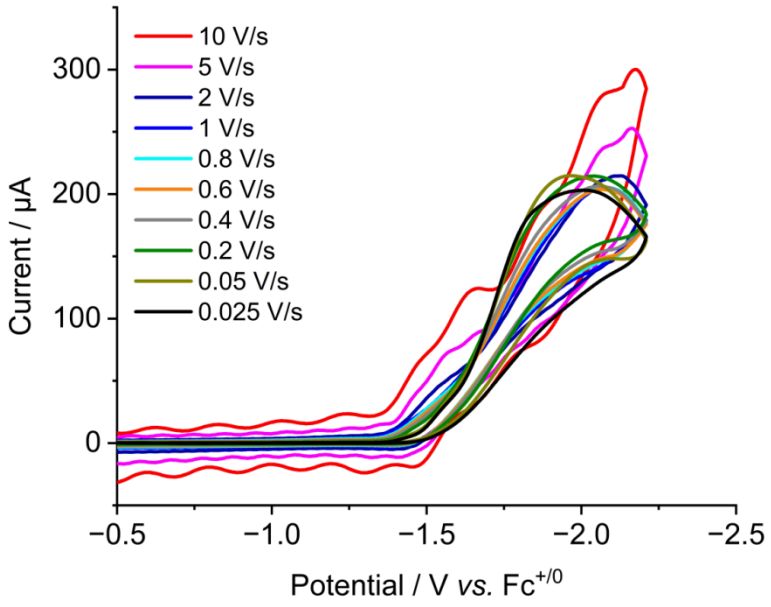

Figure S 47 Cyclic voltammograms of complex **5p** (0.5 mM) with scan rate (*v*) varied from 0.025 V/s to 10 V/s in the presence of 1.5 M TFE under CO_2. Voltammograms are taken with 0.1 M $^{n}Bu_4NPF_6$ in MeCN solution. Glassy carbon working electrode, Ag^+/Ag reference electrode, and Pt wire counter electrode.

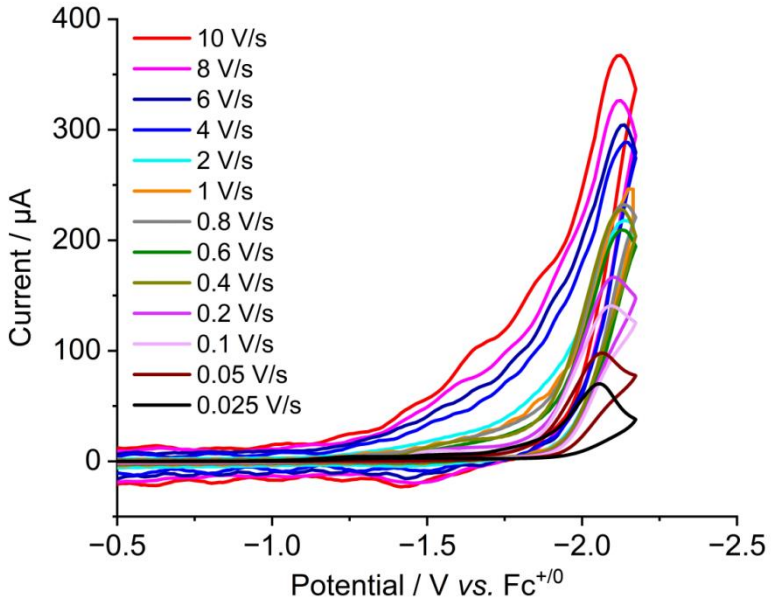

Figure S 48 Cyclic voltammograms of complex **6p** (0.5 mM) with scan rate (*v*) varied from 0.025 V/s to 10 V/s in the presence of 1.5 M TFE under CO_2. Voltammograms are taken with 0.1 M $^{n}Bu_4NPF_6$ in MeCN solution. Glassy carbon working electrode, Ag^+/Ag reference electrode, and Pt

wire counter electrode.

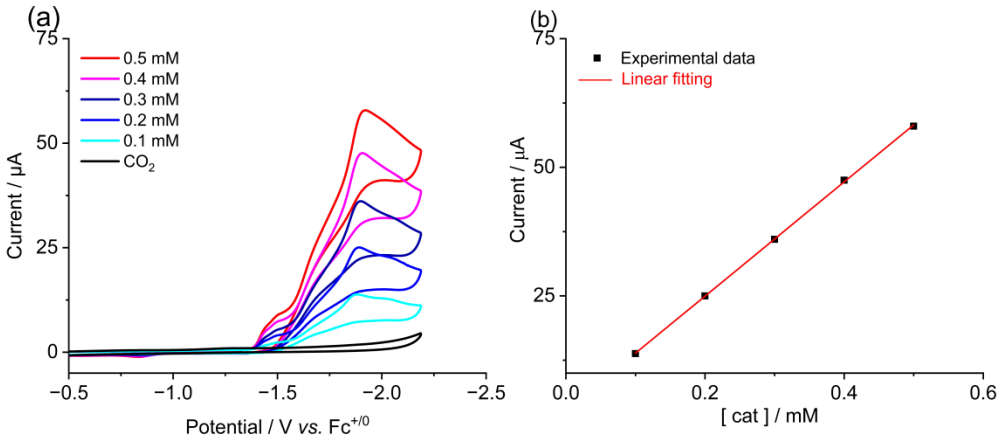

Figure S 49 (a) CVs of **1p** (0.1 – 0.5 mM) in the presence of 1.5 M TFE under CO_2; (b) The linear dependence of catalytic Current (i_{cat}) on the concentration of **1p**. Voltammograms are taken at a scan rate of 100 mV/s with 0.1 M $^{n}Bu_4NPF_6$ in MeCN solution. Glassy carbon working electrode, Ag^{+}/Ag reference electrode, and Pt wire counter electrode.

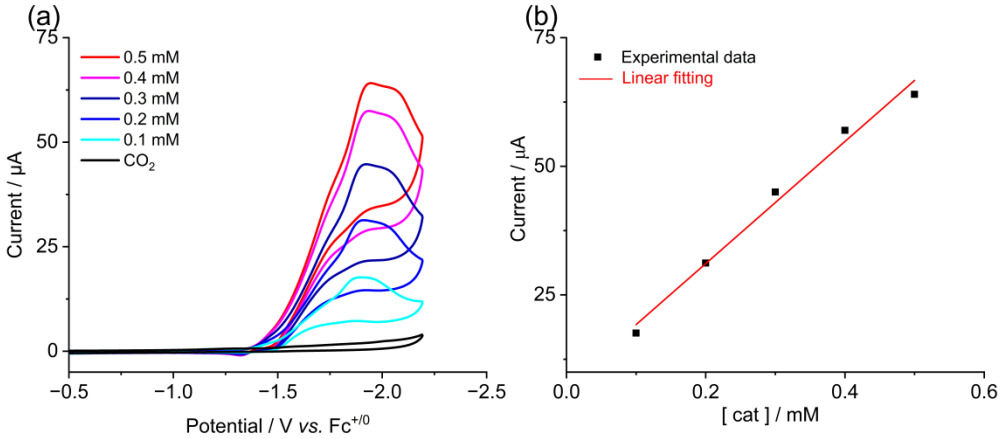

Figure S 50 (a) CVs of **2p** (0.1 – 0.5 mM) in the presence of 1.5 M TFE under CO_2; (b) The linear dependence of catalytic Current (i_{cat}) on the concentration of **2p**. Voltammograms are taken at a scan rate of 100 mV/s with 0.1 M $^{n}Bu_4NPF_6$ in MeCN solution. Glassy carbon working electrode, Ag^{+}/Ag reference electrode, and Pt wire counter electrode.

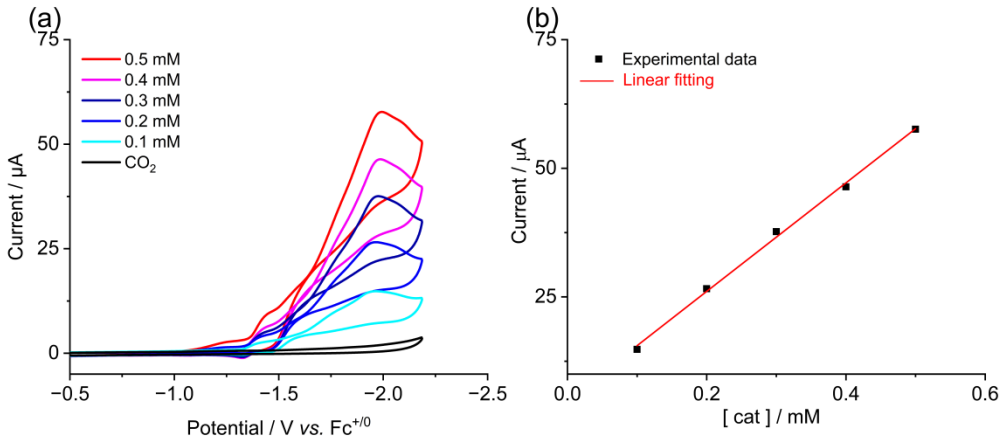

Figure S 51 (a) CVs of **3p** (0.1 – 0.5 mM) in the presence of 1.5 M TFE under CO_2; (b) The linear dependence of catalytic Current (i_{cat}) on the concentration of **3p**. Voltammograms are taken at a scan rate of 100 mV/s with 0.1 M $^{n}Bu_4NPF_6$ in MeCN solution. Glassy carbon working electrode, Ag^{+}/Ag reference electrode, and Pt wire counter electrode.

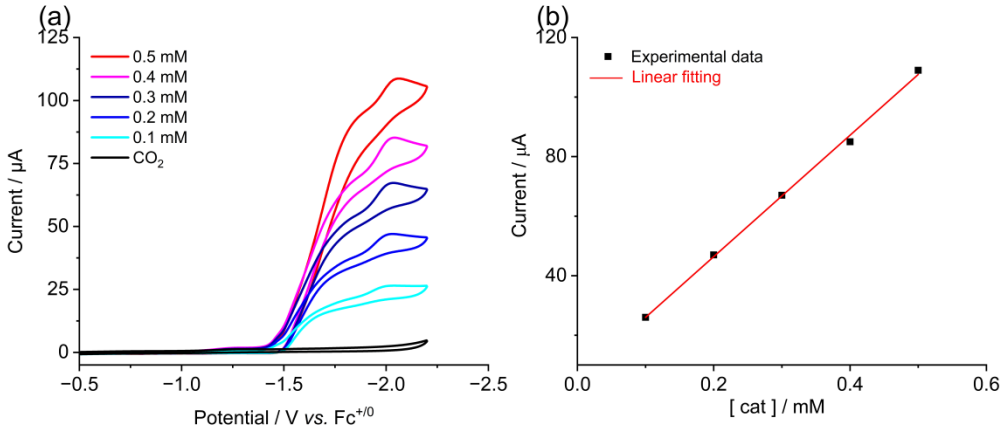

Figure S 52 (a) CVs of **4p** (0.1 – 0.5 mM) in the presence of 1.5 M TFE under CO_2; (b) The linear dependence of catalytic Current (i_{cat}) on the concentration of **4p**. Voltammograms are taken at a scan rate of 100 mV/s with 0.1 M $^{n}Bu_4NPF_6$ in MeCN solution. Glassy carbon working electrode, Ag^{+}/Ag reference electrode, and Pt wire counter electrode.

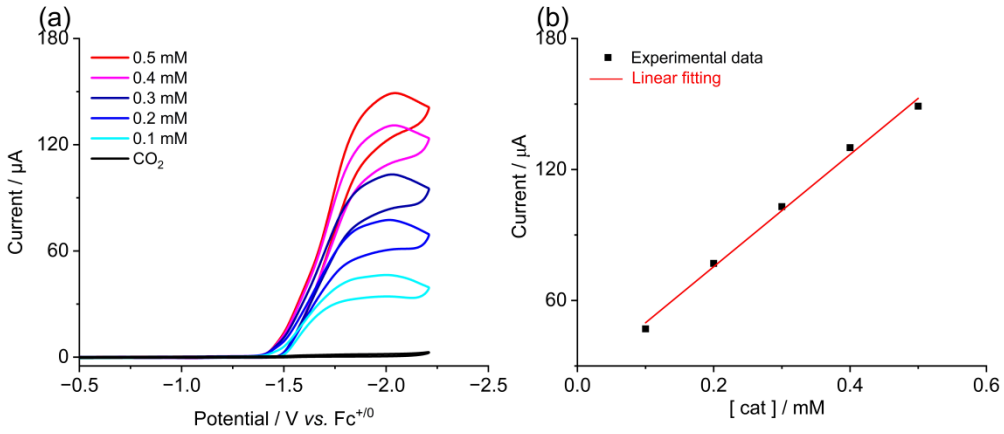

Figure S 53 (a) CVs of **5p** (0.1 – 0.5 mM) in the presence of 1.5 M TFE under CO_2; (b) The linear dependence of catalytic Current (i_{cat}) on the concentration of **5p**. Voltammograms are taken at a scan rate of 100 mV/s with 0.1 M $^{n}Bu_4NPF_6$ in MeCN solution. Glassy carbon working electrode, Ag^{+}/Ag reference electrode, and Pt wire counter electrode.

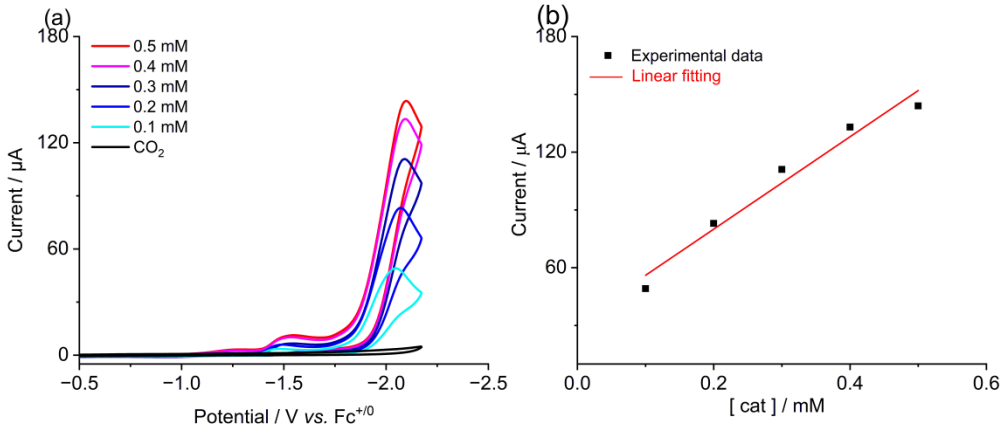

Figure S 54 (a) CVs of **6p** (0.1 – 0.5 mM) in the presence of 1.5 M TFE under CO_2; (b) The linear dependence of catalytic Current (i_{cat}) on the concentration of **6p**. Voltammograms are taken at a scan rate of 100 mV/s with 0.1 M $^{n}Bu_4NPF_6$ in MeCN solution. Glassy carbon working electrode, Ag^{+}/Ag reference electrode, and Pt wire counter electrode.

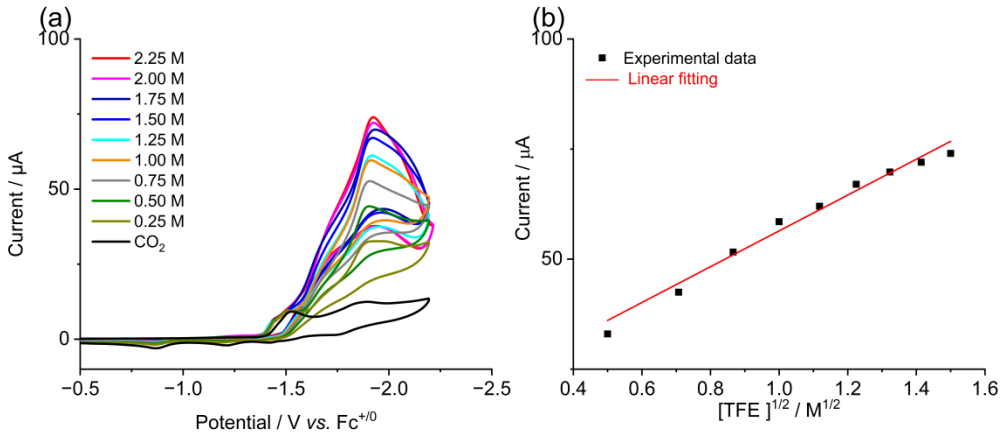

Figure S 55 (a) CVs show 0.5 mM **1p** with varied amounts of TFE under CO_2. (b) The linear dependence of catalytic Current (i_{cat}) on the square root of varied concentration of TFE. Voltammograms are taken at a scan rate of 100 mV/s with 0.1 M $^{n}Bu_4NPF_6$ in MeCN solution. Glassy carbon working electrode, Ag^+/Ag reference electrode, and Pt wire counter electrode.

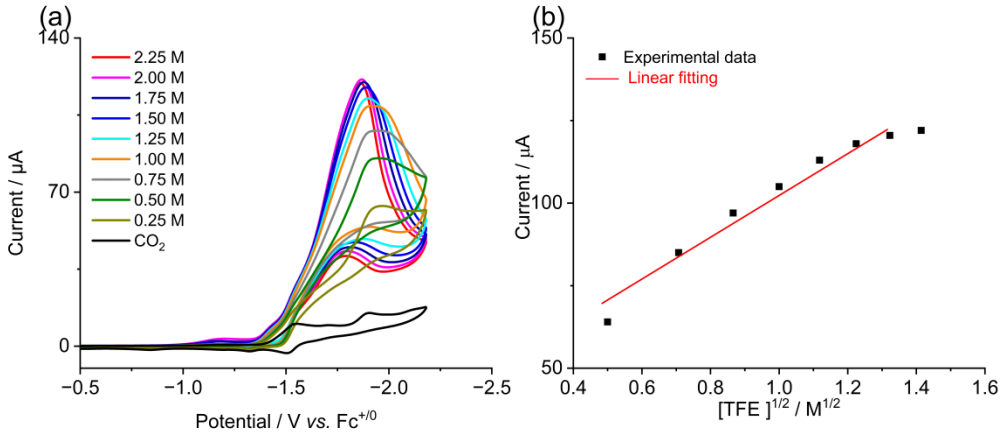

Figure S 56 (a) CVs show 0.5 mM **2p** with varied amounts of TFE under CO_2. (b) The linear dependence of catalytic Current (i_{cat}) on the square root of varied concentration of TFE. Voltammograms are taken at a scan rate of 100 mV/s with 0.1 M $^{n}Bu_4NPF_6$ in MeCN solution. Glassy carbon working electrode, Ag^+/Ag reference electrode, and Pt wire counter electrode.

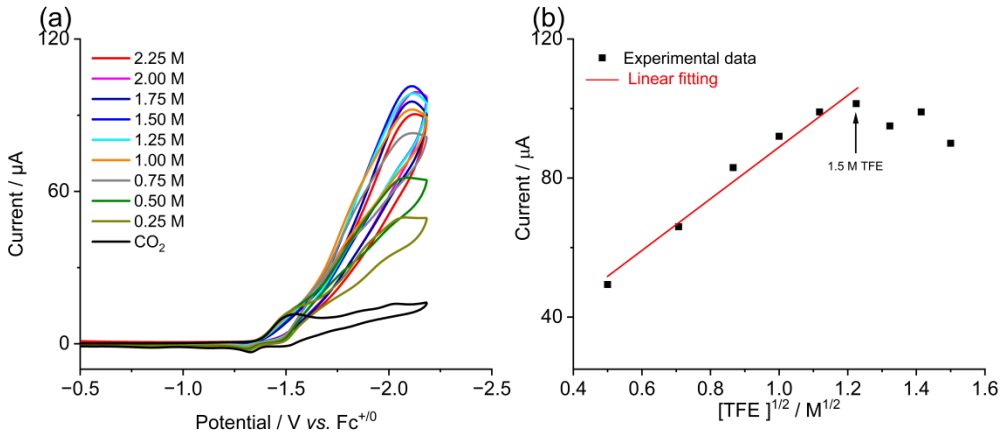

Figure S 57 (a) CVs show 0.5 mM **3p** with varied amounts of TFE under CO_2. (b) The linear dependence of catalytic Current (i_{cat}) on the square root of varied concentration of TFE. Voltammograms are taken at a scan rate of 100 mV/s with 0.1 M $^{n}Bu_4NPF_6$ in MeCN solution. Glassy carbon working electrode, Ag^+/Ag reference electrode, and Pt wire counter electrode.

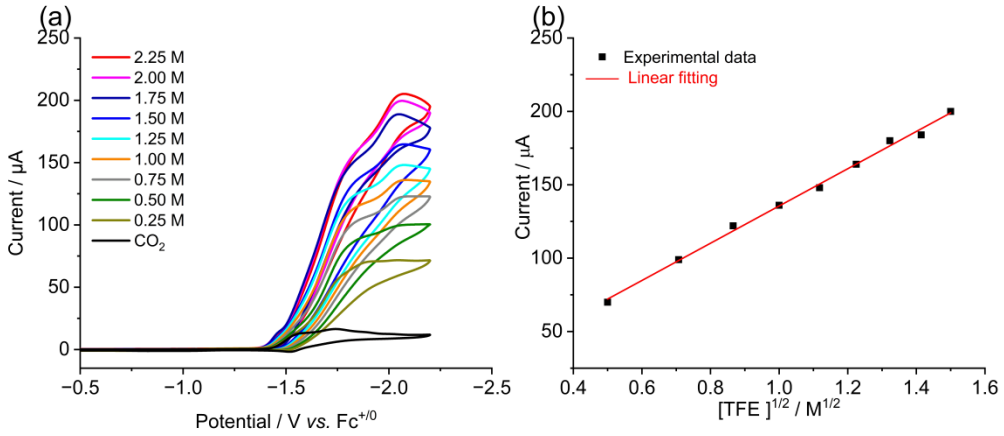

Figure S 58 (a) CVs show 0.5 mM **4p** with varied amounts of TFE under CO_2. (b) The linear dependence of catalytic Current (i_{cat}) on the square root of varied concentration of TFE. Voltammograms are taken at a scan rate of 100 mV/s with 0.1 M $^{n}Bu_4NPF_6$ in MeCN solution. Glassy carbon working electrode, Ag^+/Ag reference electrode, and Pt wire counter electrode.

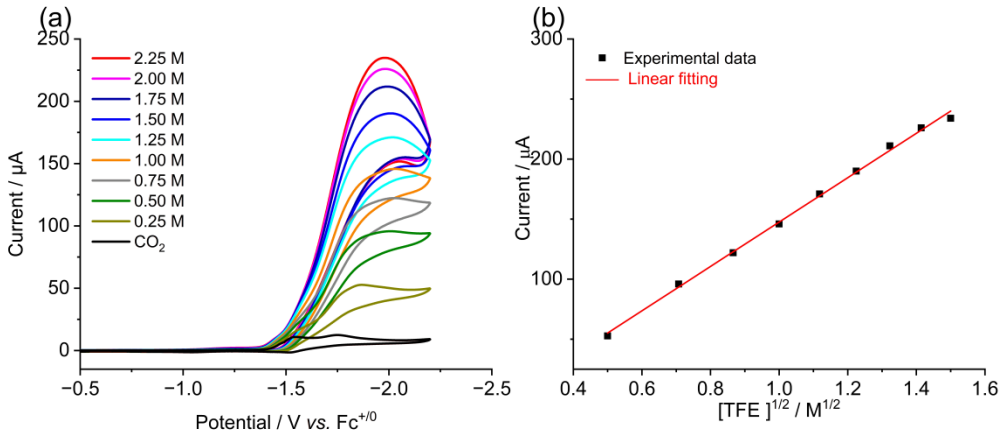

Figure S 59 (a) CVs show 0.5 mM **5p** with varied amounts of TFE under CO_2. (b) The linear dependence of catalytic Current (i_{cat}) on the square root of varied concentration of TFE. Voltammograms are taken at a scan rate of 100 mV/s with 0.1 M $^{n}Bu_4NPF_6$ in MeCN solution. Glassy carbon working electrode, Ag^+/Ag reference electrode, and Pt wire counter electrode.

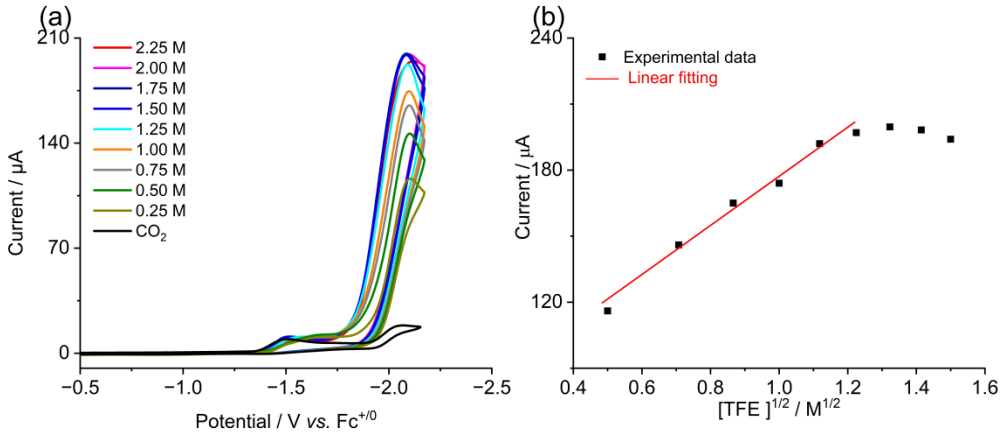

Figure S 60 (a) CVs show 0.5 mM **6p** with varied amounts of TFE under CO_2. (b) The linear dependence of catalytic Current (i_{cat}) on the square root of varied concentration of TFE. Voltammograms are taken at a scan rate of 100 mV/s with 0.1 M $^{n}Bu_4NPF_6$ in MeCN solution. Glassy carbon working electrode, Ag^+/Ag reference electrode, and Pt wire counter electrode.

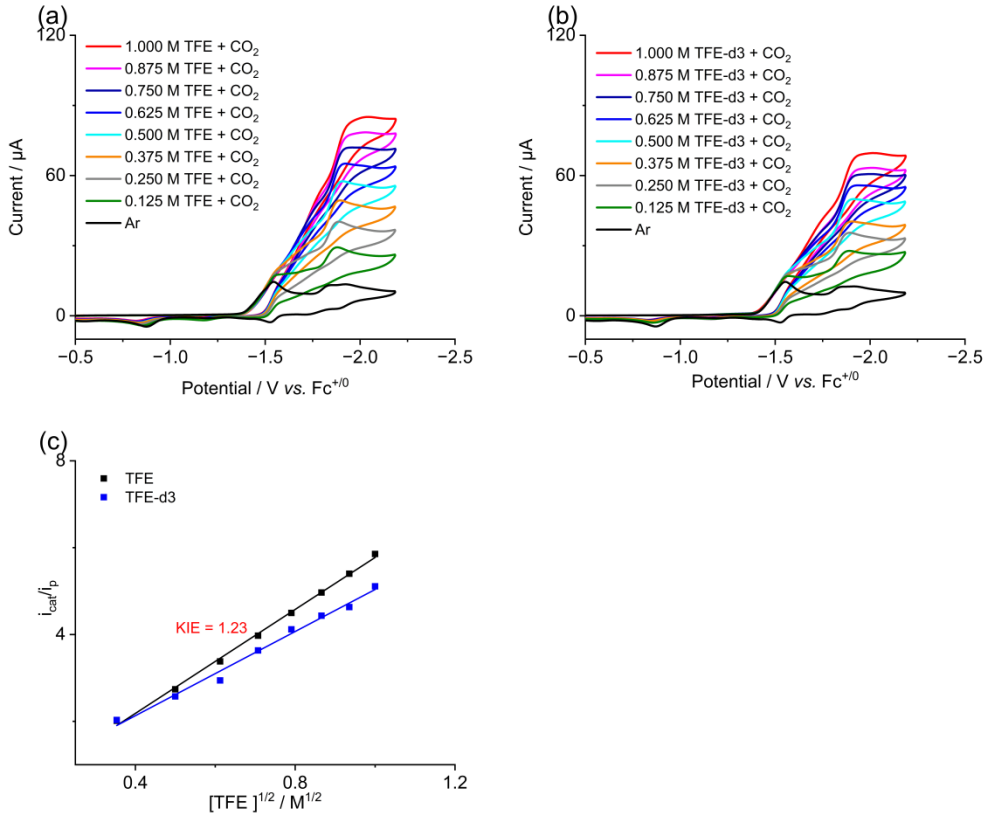

Figure S 61 (a) CVs of 0.5 mM **1p** with CO_2 in the presence of various concentration TFE. (b) CVs of 0.5 mM **1p** with CO_2 in the presence of various concentration TFE-d3. (c) The linear dependence of normalized catalytic current (i_{cat}/i_p) on the square root of the concentrations of TFE and TFE-d3.

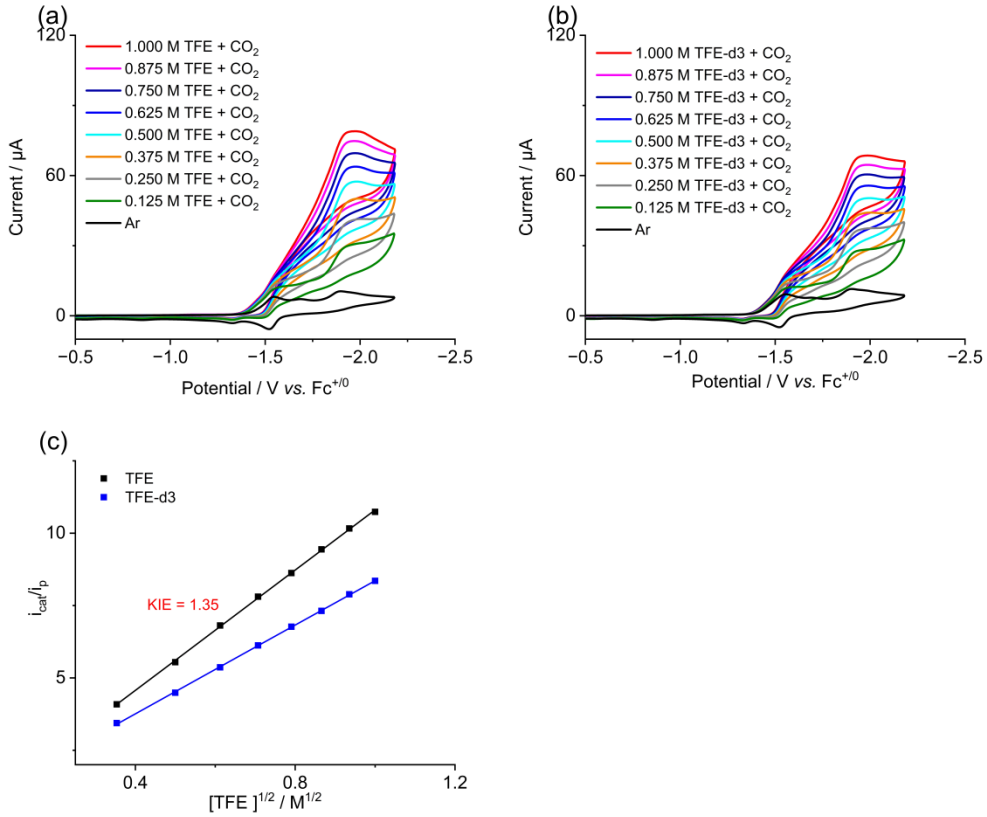

Figure S 62 (a) CVs of 0.5 mM **2p** with CO_2 in the presence of various concentration TFE. (b) CVs of 0.5 mM **2p** with CO_2 in the presence of various concentration TFE-d3. (c) The linear dependence of normalized catalytic current (i_{cat}/i_p) on the square root of the concentrations of TFE and TFE-d3.

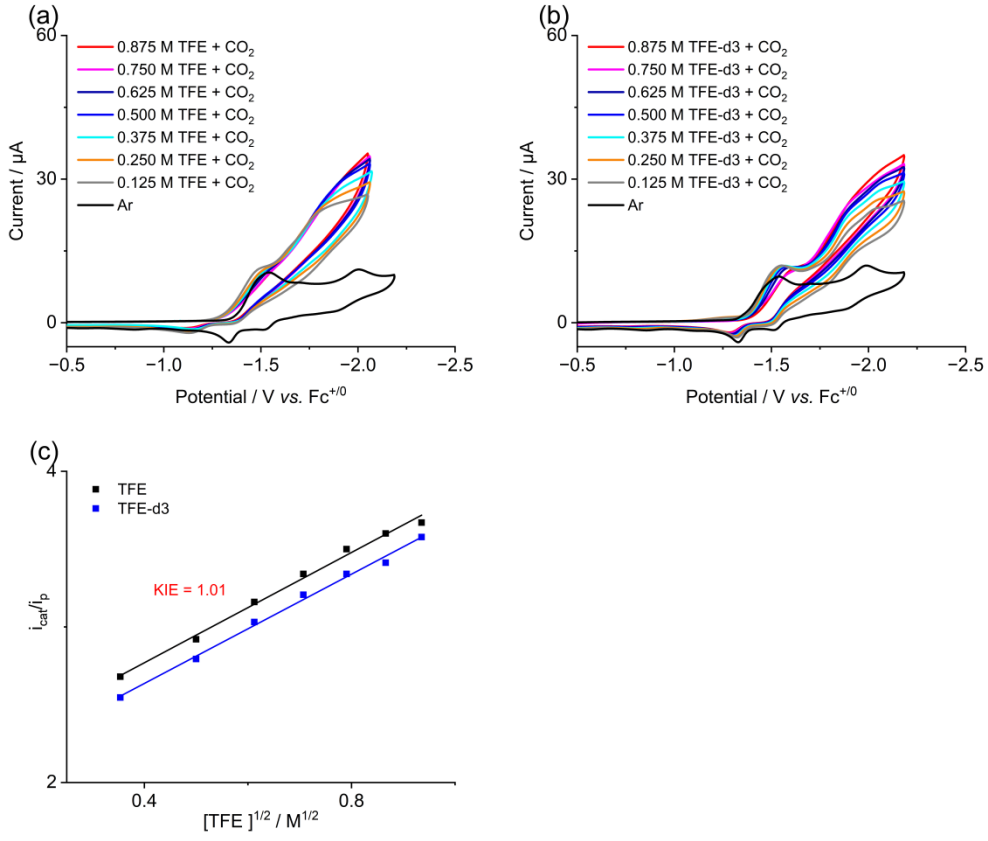

Figure S 63 (a) CVs of 0.5 mM **3p** with CO_2 in the presence of various concentration TFE. (b) CVs of 0.5 mM **3p** with CO_2 in the presence of various concentration TFE-d3. (c) The linear dependence of normalized catalytic current (i_{cat}/i_p) on the square root of the concentrations of TFE and TFE-d3.

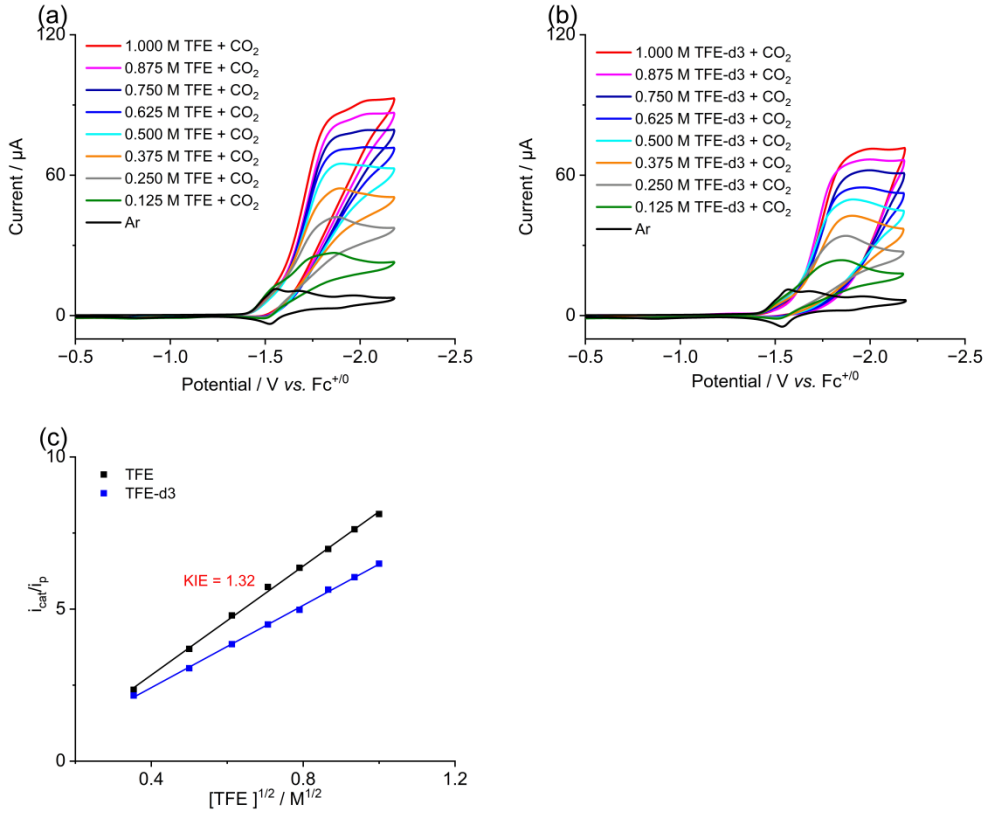

Figure S 64 (a) CVs of 0.5 mM **4P** with CO_2 in the presence of various concentration TFE. (b) CVs of 0.5 mM **4P** with CO_2 in the presence of various concentration TFE-d3. (c) The linear dependence of normalized catalytic current (i_{cat}/i_p) on the square root of the concentrations of TFE and TFE-d3.

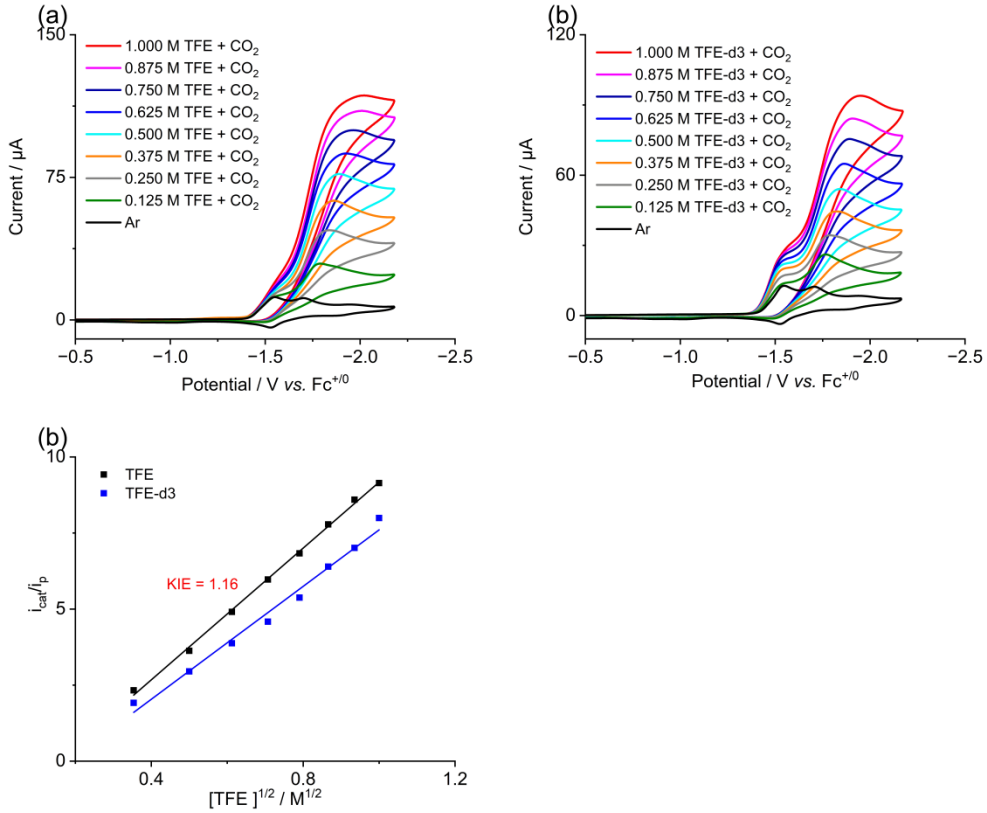

Figure S 65 (a) CVs of 0.5 mM **5p** with CO_2 in the presence of various concentration TFE. (b) CVs of 0.5 mM **5p** with CO_2 in the presence of various concentration TFE-d3. (c) The linear dependence of normalized catalytic current (i_{cat}/i_p) on the square root of the concentrations of TFE and TFE-d3.

10. Details for Foot-of-the-Wave Analysis (FOWA) and determination of kobs.

Foot-of-the-Wave Analysis was applied to cyclic voltammetry measurements as described by Savéant and coworkers (*Science.*, 2012, **338**, 90-94;) in order to determine k_{obs} = TOF under the specified conditions. At the outset of each experiment, a cyclic voltammogram was measured of catalyst alone under inert atmosphere in the absence of proton source, from which E^0_{cat} could be determined. The half of the peak height of the formal **1** / (**1**$^{2-}$ - Br$^-$) couple, i^0_p, was determined by taking the difference between peak cathodic current and baseline current before this couple.

$$\frac{i}{i_p^0} = \frac{2.24\sqrt{\frac{k_{obs}}{fv}}}{1 + e^{[f(E-E^0_{cat})]}}$$

where i is the catalytic current, E is the potential, v is the scan rate (V/s), k_{obs} is the observed rate constant, and f = F/RT = 38.94 V^{-1}. Thus, a "FOW" plot of $\frac{i}{i_p^0}$ *versus* $\frac{1}{1+e^{[f(E-E^0_{cat})]}}$ yields a straight line with slope $2.24\sqrt{\frac{k_{obs}}{fv}}$, from which k_{obs} may be determined.

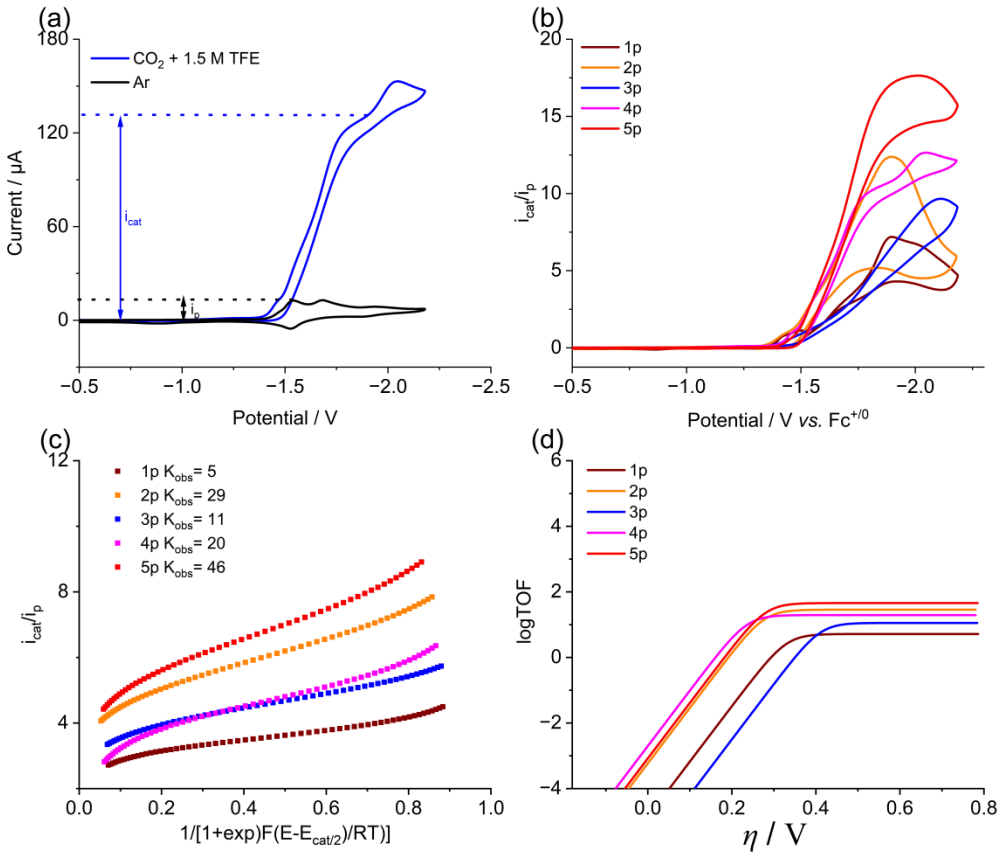

Figure S 66 (a) CVs of 0.5 mM **4p** under Ar in the absence of TFE (black line), under CO_2 in the presence of 1.5 M TFE (blue line). Voltammograms are taken at a scan rate of 100 mV/s with 0.1 M $^{n}Bu_4NPF_6$ in MeCN solution. (b) Cyclic voltammetry of **1p - 5p** in the potential domain of the catalytic CO_2 reduction wave in acetonitrile + 0.1 M $^{n}Bu_4NPF_6$ + 1.5 M TFE, at 0.1 V/s under 1 atm. CO_2 (catalyst concentration is 0.5 mM). The current, i_{cat} is normalized against the peak current of the reversible one-electron reversible wave, i_p obtained at the same scan rate (0.1 V/s). (c) Under the conditions of 1.5 M TFE and saturated CO_2, during the CO_2 reduction stage, foot-of-the-wave analysis of **1p - 5p** under equivalent experimental conditions with a linear fit extrapolated from (E - $E_{cat/2}$) at a scan rates of 0.1 V/s. (d) Catalytic Tafel plots of **1p - 5p** in the presence of of 1.5 M TFE under CO_2. Voltammograms are taken with 0.1 M $^{n}Bu_4NPF_6$ in MeCN solution. Glassy carbon working electrode, Ag^+/Ag reference electrode, and Pt wire counter electrode.

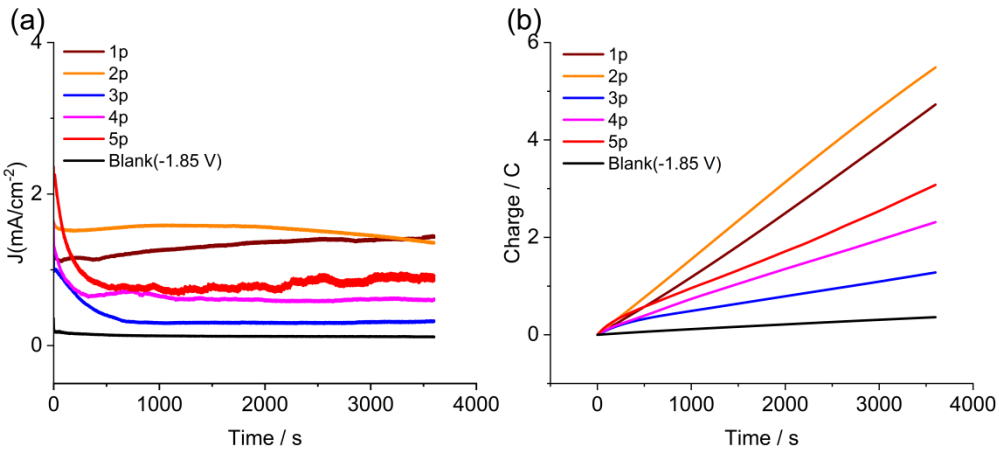

Figure S 67 (a) Controlled potential electrolysis at -1.85 V *vs.* $Fc^{+/0}$ in the presence and absence of 0.5 mM **1p - 5p** under CO_2 in the presence of 1.5 M TFE. (b) The charge integration after electrolysis (-1.85 V *vs.* $Fc^{+/0}$) for **1p - 5p**

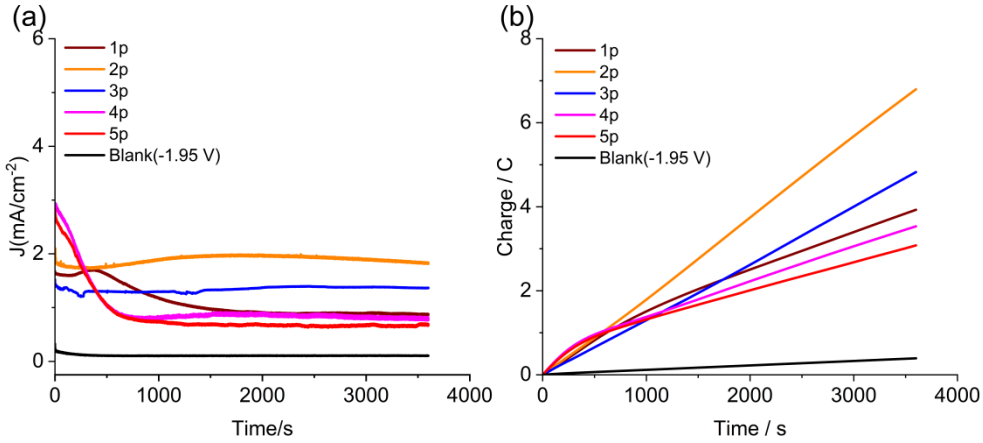

Figure S 68 (a) Controlled potential electrolysis at -1.95 V *vs.* $Fc^{+/0}$ in the presence and absence of 0.5 mM **1p - 5p** under CO_2 in the presence of 1.5 M TFE. (b) The charge integration after electrolysis (-1.95 V *vs.*$Fc^{+/0}$) for **1p - 5p**

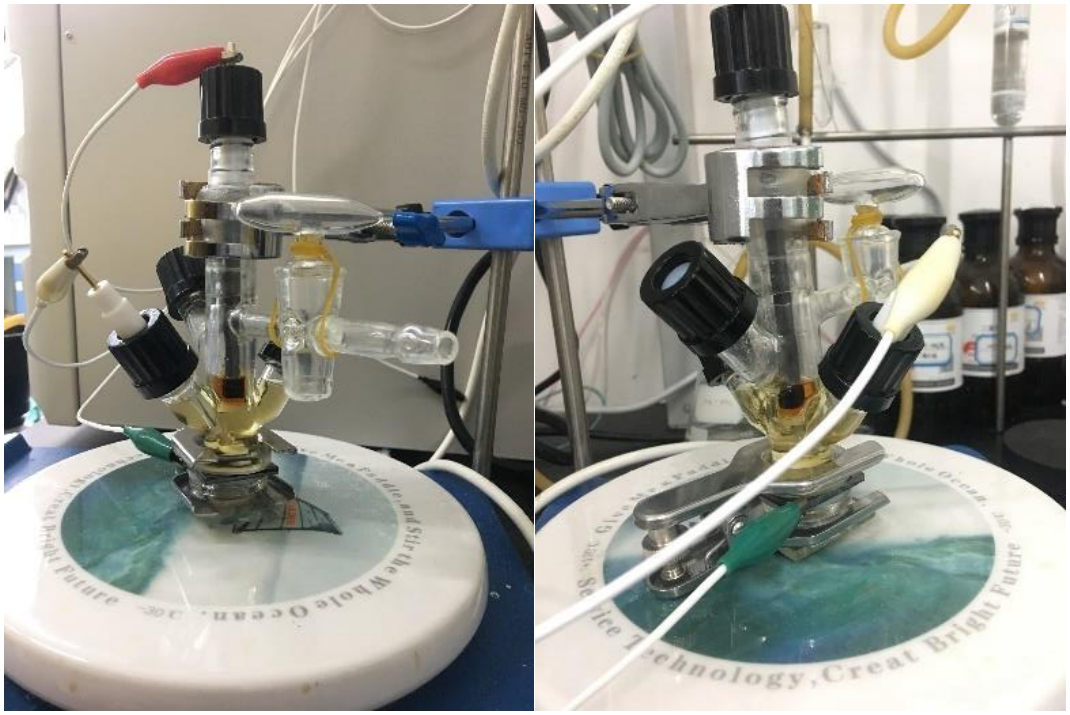

Figure S 69 the custom cell designed in our laboratory.

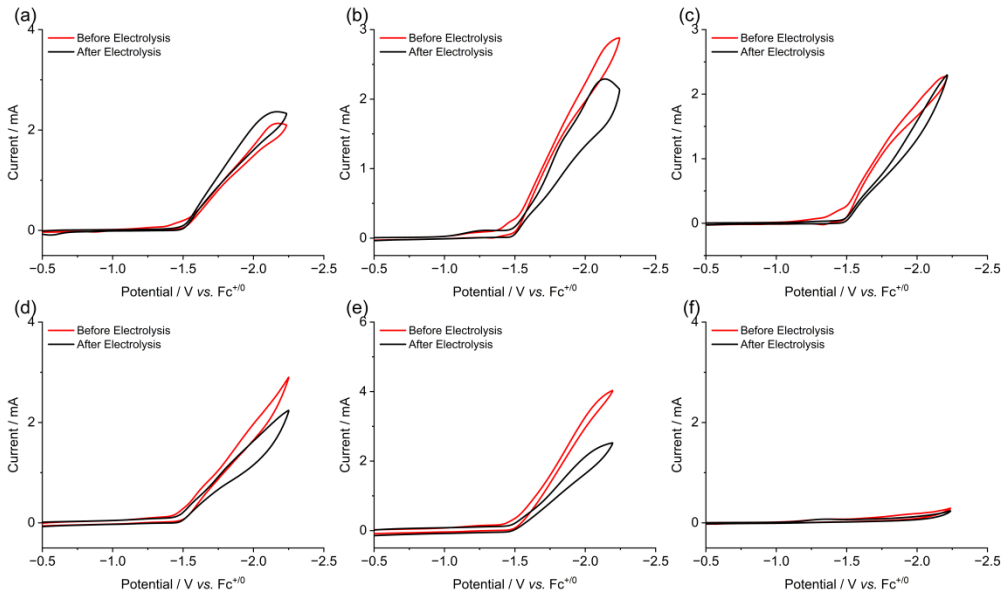

Figure S 70 (a) Cyclic voltammograms show 0.5 mM **1p** before and after electrolysis at -1.85 V *vs.* $Fc^{+/0}$ under CO_2 in the presence of 1.5 M TFE. (b) Cyclic voltammograms show 0.5 mM **2p** before and after electrolysis at -1.85 V *vs.* $Fc^{+/0}$ under CO_2 in the presence of 1.5 M TFE. (c) Cyclic voltammograms show 0.5 mM **3p** before and after electrolysis at -1.85 V *vs.* $Fc^{+/0}$ under CO_2 in the presence of 1.5 M TFE. (d) Cyclic voltammograms show 0.5 mM **4p** before and after electrolysis at -1.85 V *vs.* $Fc^{+/0}$ under CO_2 in the presence of 1.5 M TFE. (e) Cyclic voltammograms show 0.5 mM **5p** before and after electrolysis at -1.85 V *vs.* $Fc^{+/0}$ under CO_2 in the presence of 1.5 M TFE. (f) Cyclic voltammograms show the blank before and after electrolysis at -1.85 V *vs.* $Fc^{+/0}$ under CO_2 in the presence of 1.5 M TFE.

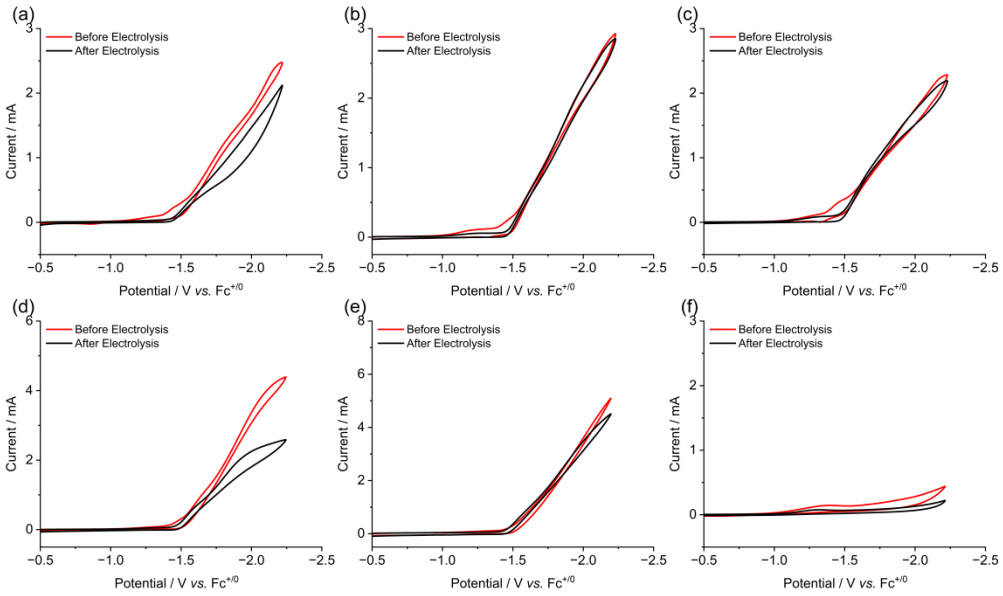

Figure S 71 (a) Cyclic voltammograms show 0.5 mM **1p** before and after electrolysis at -1.95 V *vs.* $Fc^{+/0}$ under CO_2 in the presence of 1.5 M TFE. (b) Cyclic voltammograms show 0.5 mM **2p** before and after electrolysis at -1.95 V *vs.* $Fc^{+/0}$ under CO_2 in the presence of 1.5 M TFE. (c) Cyclic voltammograms show 0.5 mM **3p** before and after electrolysis at -1.95 V vs. $Fc^{+/0}$ under CO_2 in the presence of 1.5 M TFE. (d) Cyclic voltammograms show 0.5 mM **4p** before and after electrolysis at -1.95 V *vs.* $Fc^{+/0}$ under CO_2 in the presence of 1.5 M TFE. (e) Cyclic voltammograms show 0.5 mM **5p** before and after electrolysis at -1.95 V *vs.* $Fc^{+/0}$ under CO_2 in the presence of 1.5 M TFE. (f) Cyclic voltammograms show the blank before and after electrolysis at -1.95 V *vs.* $Fc^{+/0}$ under CO_2 in the presence of 1.5 M TFE.

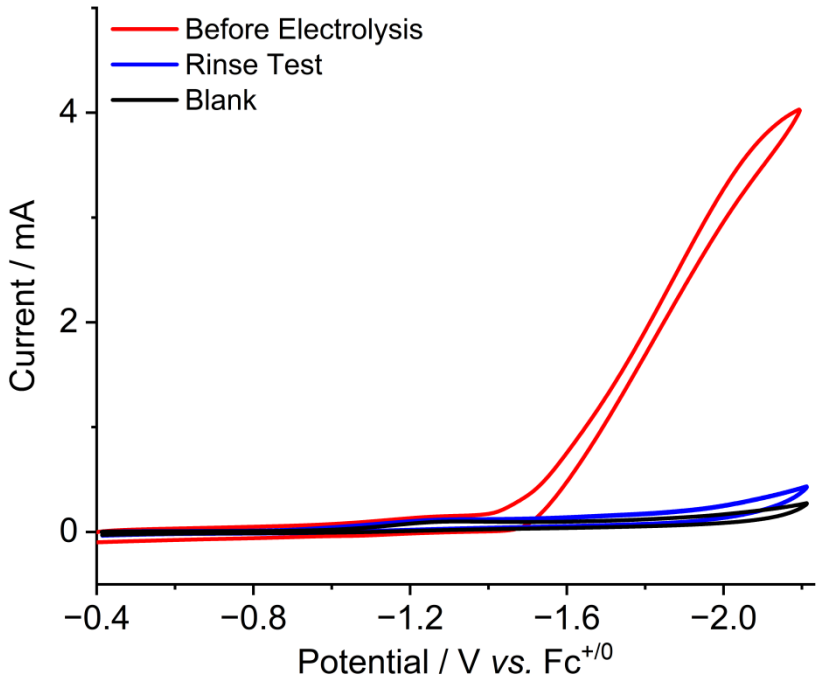

Figure S 72 (a) Cyclic voltammograms show a "rinse test" following 0.5 mM **5p** after electrolysis at -1.85 V *vs.* $Fc^{+/0}$ under CO_2 in the presence of 1.5 M TFE.

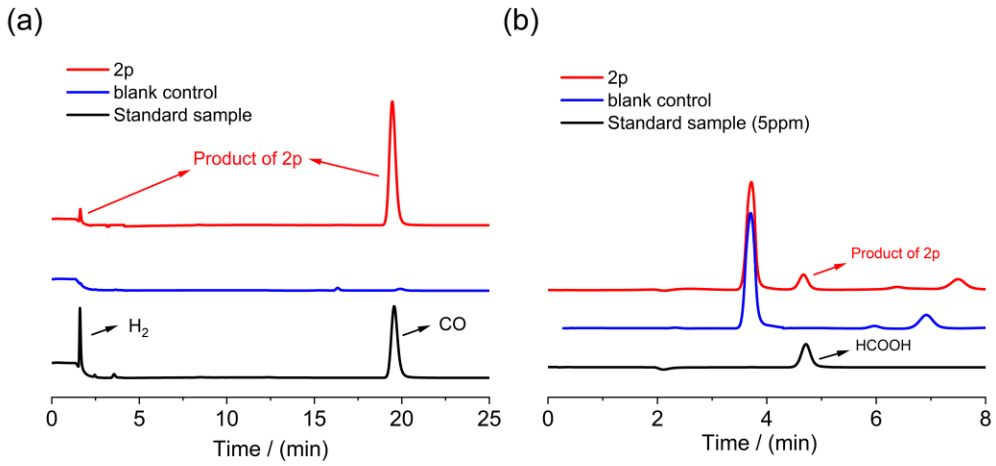

Figure S 73 (a) The gas products channel of **2p** (red line), control experiments (blue line) and standard sample (black line). (b) The liquid products channel of **2p**, control experiments (blue line) and standard sample (black line).

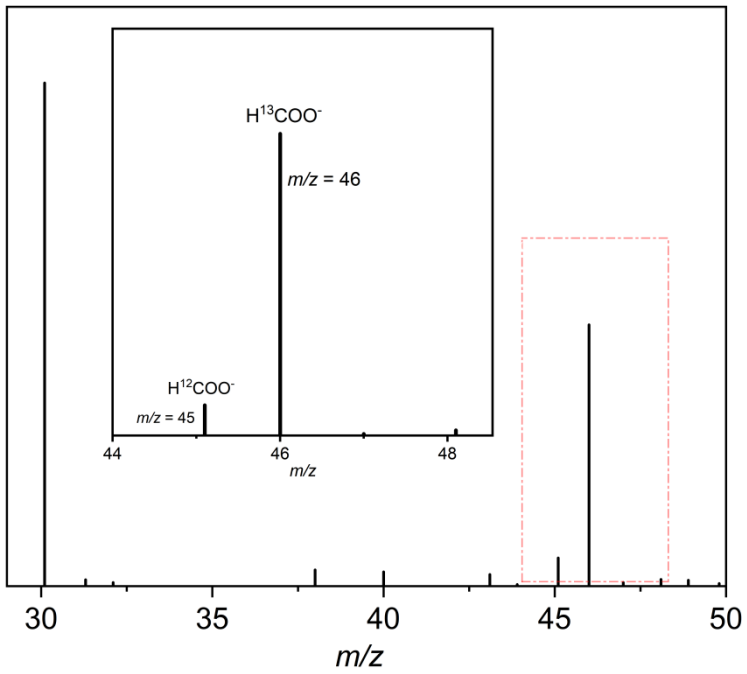

Figure S 74 Mass spectra of the electrolyte resulting from electrolysis of the $^{13}CO_2$ saturated-MeCN solution containing 0.5 mM **2p**, 1.5 M TFE, and 0.1 M $^{n}Bu_4NPF_6$ at -1.85 V over 1 h.

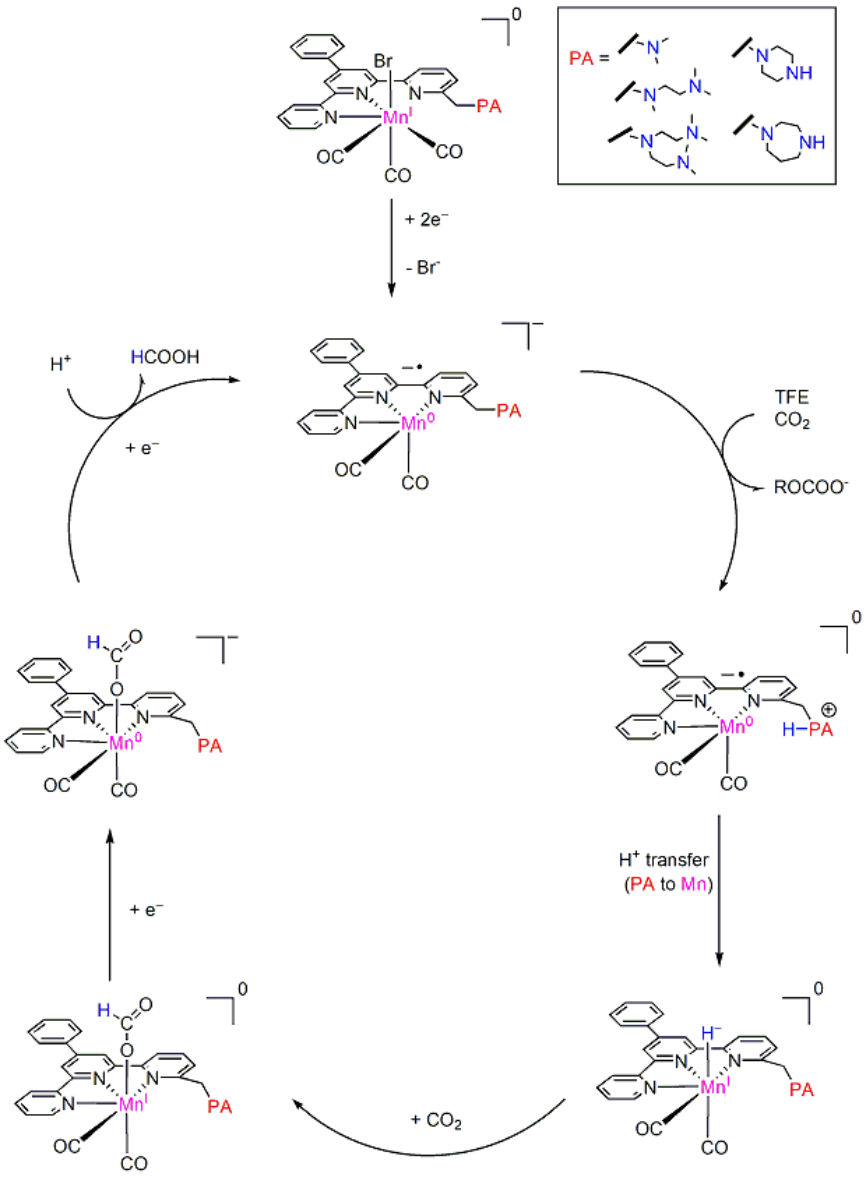

Scheme S 14 proposed catalytic cycle for the reduction of CO_2 to HCOOH.

Table S 1 Quantitative analysis of the CPE results of **1p-5p**

Complex	Proton source(1.5 M)	Charge(C)	E (V *vs* $Fc^{+/0}$)	FE%(H_2:CO:HCOOH)			TON
1p	TFE	4.729	-1.85	1.7	11.7	91.9	5.26
2p		5.279		6.7	15.2	83.8	5.89
3p		1.280		9.6	17.5	81.8	1.24
4p		2.313		2.3	18.9	84.7	2.44
5p		3.078		1.0	13.1	93.2	3.33
Blank		0.215		/	/	/	/
1p		3.929	-1.95	1.9	14.3	92.4	4.33
2p		6.797		7.7	15.9	82.1	7.67
3p		4.827		8.1	18.9	79.2	5.38
4p		3.536		3.8	18.6	85.9	3.88
5p		3.081		1.5	14.2	90.6	3.34
Blank		0.208		/	/	/	/

Table S 2 Summary of IR-SEC data of complexes **1p-6p.**

States	Wavenumbers / cm^{-1}
1p	2023, 1931, 1918
1	1898, 1862
[1^{2-}-Br]	1828, 1762
2p	2025, 1930, 1919
2/[2^{2-}-Br]	1902, 1864/ 1826, 1760
[2^{2-}-Br]	1826, 1760
3p	2026, 1931, 1919
3/[3^{2-}-Br]	1901, 1862/ 1829, 1761
4p	2023, 1930, 1921
4	1902, 1858
[4^{2-}-Br]	1830, 1762
5p	2024, 1931, 1918
5	1901, 1863
[5^{2-}-Br]	1827, 1760
6p	2018,1931,1901
[$6p^{2-}$-Br]	1903,1806

Table S 3 Performance comparison data of **2p** and **5p** with other catalysts.

Catalyst	Solvent	FE_{COOH}%	$TOF_{max}(s^{-1})$	η (V)	Refs
2p (This work)	MeCN +1.5 M TFE	83 ± 5	29	0.28	/
5p (This work)	MeCN +1.5 M TFE	93 ± 5	46	0.275	/
fac-[Mn(bpy-NEt_2)$(CO)_3$Br]	MeCN +2.0 M TFE	63	87	0.27	1
fac-[Mn(4,4'-(Ph-NEt_2)$_2$-bpy)$(CO)_3$Br]	MeCN + 2.0 M TFE	70	110	0.30	1
[FeN_5]	95% MeCN + 5% H_2O	77 ± 3	0.29	0.31	2
$[Fe_4N(CO)_{12}]^-$	95% MeCN + 5% H_2O	94 ± 3	10	0.44	3
[μ - C_6H_4 - 1,2-(κ^2 - S)$_2$][$Fe_2(CO)_6$]	MeCN + 1.5 M MeOH	81	195	0.95	4
(POCOP)IrH_2	95% MeCN + 5% H_2O	85	20	0.68	5
(PN^HP)IrH_3	88% MeCN + 12% H_2O	97	0.56	0.33	6
CpCo($P^{Cy}_2N^{Bn}_2$)I	DMF + 1.1 M H_2O	92 ± 8	70	0.65	7
CpCo($P^{Ph}_2N^{Ph}_2$)I	DMF + 1.1 M H_2O	98 ± 8	650	0.80	7

Reference

[1] M. H. Rønne, D. Cho, M. R. Madsen, J. B. Jakobsen, S. Eom, É. Escoudé, H. C. D. Hammershøj, D. U. Nielsen, S. U. Pedersen, M. Baik, T. Skrydstrup and K. Daasbjerg, *J. Am. Chem. Soc.*, 2020, **142**, 3615–3623.

[2] L. Chen, Z. Guo, X.-G. Wei, C. Gallenkamp, J. Bonin, E. Anxolabéhère-Mallart, K.-C. Lau, T.-C. Lau and M. Robert, *J. Am. Chem. Soc.*, 2015, **137**, 10918–10921.

[3] A. Taheri, E. J. Thompson, J. C. Fettinger and L. A. Berben, *ACS Catal.*, 2015, **5**, 7140–7151.

[4] M. Cheng, Y. Yu, X. Zhou, Y. Luo and M. Wang, *ACS Catal.*, 2019, **9**, 768–774.

[5] P. Kang, C. Cheng, Z. Chen, C. K. Schauer, T. J. Meyer and M. Brookhart, *J. Am. Chem. Soc.*, 2012, **134**, 5500–5503.

[6] S. T. Ahn, E. A. Bielinski, E. M. Lane, Y. Chen, W. H. Bernskoetter, N. Hazari and G. T. R. Palmore, *Chem. Commun.*, 2015, **51**, 5947–5950.

[7] S. Roy, B. Sharma, J. Pécaut, P. Simon, M. Fontecave, P. D. Tran, E. Derat and V. Artero, *J. Am. Chem. Soc.*, 2017, **139**, 3685–3696.